Dual control by Cdk1 phosphorylation of the budding yeast APC/C ubiquitin ligase activator Cdh1

Sebastian Höckner, Lea Neumann-Arnold, and Wolfgang Seufert*
Department of Genetics, University of Regensburg, D-93040 Regensburg, Germany

ABSTRACT **The antagonism between cyclin-dependent kinases (Cdks) and the ubiquitin ligase APC/C-Cdh1 is central to eukaryotic cell cycle control. APC/C-Cdh1 targets cyclin B and other regulatory proteins for degradation, whereas Cdks disable APC/C-Cdh1 through phosphorylation of the Cdh1 activator protein at multiple sites. Budding yeast Cdh1 carries nine Cdk phosphorylation sites in its N-terminal regulatory domain, most or all of which contribute to inhibition. However, the precise role of individual sites has remained unclear. Here, we report that the Cdk phosphorylation sites of yeast Cdh1 are organized into autonomous subgroups and act through separate mechanisms. Cdk sites 1–3 had no direct effect on the APC/C binding of Cdh1 but inactivated a bipartite nuclear localization sequence (NLS) and thereby controlled the partitioning of Cdh1 between cytoplasm and nucleus. In contrast, Cdk sites 4–9 did not influence the cell cycle–regulated localization of Cdh1 but prevented its binding to the APC/C. Cdk sites 4–9 reside near two recently identified APC/C interaction motifs in a pattern conserved with the human Cdh1 orthologue. Thus a Cdk-inhibited NLS goes along with Cdk-inhibited APC/C binding sites in yeast Cdh1 to relay the negative control by Cdk1 phosphorylation of the ubiquitin ligase APC/C-Cdh1.**

Monitoring Editor
Mark J. Solomon
Yale University

Received: Nov 17, 2015
Revised: May 4, 2016
Accepted: May 18, 2016

INTRODUCTION

Phosphorylation by cyclin-dependent kinases (Cdks) and protein degradation by the ubiquitin proteasome system are key mechanisms by which the events of the eukaryotic cell division cycle are coordinated (King *et al.*, 1996). These two pathways serve to phosphorylate or remove several critical cell cycle regulatory proteins in a precise temporal pattern (Pines, 1999; Sullivan and Morgan, 2007; Enserink and Kolodner, 2010; Bassermann *et al.*, 2014). In fact, these mechanisms are closely linked, in that ubiquitin-mediated proteolysis underlies the periodic accumulation of cyclins and serves to down-regulate Cdk activity. Cdks, on the other hand, may promote or inhibit ubiquitin-mediated proteolysis through phosphorylation of substrate proteins or components of the ubiquitination machinery (Petroski and Deshaies, 2005; Bloom and Cross, 2007; Teixeira and Reed, 2013).

The anaphase-promoting complex/cyclosome (APC/C) is a large E3 ubiquitin ligase with essential functions during mitosis and G1 (Peters, 2006). The APC/C recognizes its substrates with the help of two structurally related activator proteins, Cdc20 and Cdh1 (Barford, 2011; Primorac and Musacchio, 2013). These activators contain a conserved WD40 domain, which folds into a seven-bladed β-propeller and provides receptor sites for specific degradation signals present in APC/C substrates, such as D- and KEN-boxes (Glotzer *et al.*, 1991; Pfleger and Kirschner, 2000; Chao, Kulkarni, *et al.*, 2012; Tian, Li, *et al.*, 2012; He, Chao, *et al.*, 2013). In addition, the Cdc20 and Cdh1 activators use specific sequence motifs, namely the conserved C-box and C-terminal IR motif (Schwab *et al.*, 2001; Vodermaier, Gieffers, *et al.*, 2003), as well as the KILR motif identified in human Cdc20 (Zhang and Lees, 2001; Izawa and Pines, 2012), to bind the APC/C core. These activators not only recruit substrates to the APC/C, but they also stimulate its ubiquitination activity (Kimata *et al.*, 2008; Labit *et al.*, 2012), probably by a conformational change in the complex (Herzog *et al.*, 2009; Chang, Zhang, *et al.*, 2014) and increased E2 binding (Kelly, Wickliffe, Song, *et al.*, 2014;

This article was published online ahead of print in MBoC in Press (http://www.molbiolcell.org/cgi/doi/10.1091/mbc.E15-11-0787) on May 25, 2016.

*Address correspondence to: Wolfgang Seufert (Wolfgang.Seufert@ur.de).

Abbreviations used: APC/C, anaphase-promoting complex/cyclosome; Cdk, cyclin-dependent kinase; CTD, C-terminal domain; DIC, differential interference contrast; GFP, green fluorescent protein; NLS, nuclear localization sequence; Noc, nocodazole; NTD, N-terminal domain; ROI, region of interest; WCE, whole-cell extract.

Van Voorhis and Morgan, 2014). Cdc20 activates the APC/C during metaphase and, besides initiating cyclin destruction (Clute and Pines, 1999; Shirayama *et al.*, 1999; Yeong *et al.*, 2000; Wasch and Cross, 2002), primarily targets the anaphase inhibitor securin for degradation to promote sister-chromatid separation (Cohen-Fix *et al.*, 1996; Waizenegger *et al.*, 2000). At the end of mitosis, Cdc20 is replaced by the second activator, Cdh1, which activates the ubiquitin ligase against several mitotic regulators to facilitate mitotic exit (Peters, 2006). Among others, Cdh1 completes the degradation of mitotic cyclins and keeps their protein levels low during the following G1 phase to prevent unscheduled S-phase entry (Brandeis and Hunt, 1996; Irniger and Nasmyth, 1997; Schwab *et al.*, 2001; Wasch and Cross, 2002). Beyond its important function in dividing cells, APC/C-Cdh1 is also active in postmitotic cells of higher eukaryotes, with possible roles in controlling differentiation and metabolism, as well as in neuronal survival (Eguren *et al.*, 2011; Almeida, 2012). Indeed, studies suggest that down-regulation of APC/C-Cdh1 activity might contribute to neuronal cell death in the development of neurodegenerative disorders (Almeida *et al.*, 2005; Maestre *et al.*, 2008).

Activation of the APC/C by Cdc20 and Cdh1 is tightly regulated to ensure precise and timely degradation of its substrates. This regulation occurs at multiple levels and includes pseudosubstrate inhibitors, Cdc20 turnover, and phosphorylation by Cdk (Pesin and Orr-Weaver, 2008; Primorac and Musacchio, 2013). Besides other mechanisms that partly differ among organisms, phosphorylation by Cdk is primarily responsible for controlling APC/C activation by Cdh1 and, in addition, helps establish the ordered binding of Cdc20 and Cdh1 to the APC/C. In early mitosis, phosphorylation of APC/C subunits by Cdks supports the binding of Cdc20 (Kramer *et al.*, 2000; Rudner and Murray, 2000; Kraft *et al.*, 2003). At the same time, Cdk phosphorylation of Cdh1 prevents its association with the APC/C (Zachariae, Schwab, *et al.*, 1998; Jaspersen *et al.*, 1999; Lukas *et al.*, 1999; Blanco *et al.*, 2000; Kramer *et al.*, 2000). At the end of mitosis, APC/C-Cdc20–dependent reduction of Cdk activity enables phosphatases to dephosphorylate Cdh1 (Wurzenberger and Gerlich, 2011), which then binds and activates the APC/C until the end of G1 phase. Then, increasing levels of G1/S cyclins, which are not targeted by the APC/C, result in phosphorylation and inactivation of Cdh1 by Cdk. This mutual inhibition between Cdh1 and Cdks is an important feature in cell cycle control for accurate switches between states of high and low Cdk activity.

In budding yeast, phosphorylation by Cdk1 was also reported to cause cytoplasmic localization of otherwise nuclear Cdh1 (Jaquenoud *et al.*, 2002). Given that APC/C-Cdh1 activity was recently shown to be restricted to the nuclear compartment in *Saccharomyces cerevisiae* (Arnold, Höckner, *et al.*, 2015), Cdh1 translocation to the cytoplasm is likely to contribute to inactivation of APC/C-Cdh1. Although subcellular localization of the APC/C, its activators, or substrates might serve as an important mechanism for spatial control of APC/C-Cdh1 activity, this aspect has received attention only recently (Sivakumar and Gorbsky, 2015). The N-terminal domain (NTD) of yeast Cdh1, similar to Cdh1 orthologues in other organisms, contains multiple sites that match either the minimal (S/TP) or full consensus sequence (S/TPxK/R) for phosphorylation by Cdk1. Proteomic studies show that Cdh1 is indeed phosphorylated at these Cdk consensus sites in vivo (Hall *et al.*, 2004; Holt, Tuch, Villén, *et al.*, 2009; Swaney *et al.*, 2013). Because most previous experiments were performed with a *CDH1* mutant lacking all Cdk sites, the relevance of individual Cdk sites in Cdh1 for its localization and APC/C association has been unresolved. In this study, we used live-cell imaging to analyze green fluorescent protein (GFP) fusion constructs of truncated or mutated versions of Cdh1 to determine localization sequences. Moreover, we analyzed Cdh1 mutants lacking different Cdk sites for their subcellular localization and APC/C binding to gain a deeper understanding of how Cdk1 phosphorylation controls the function of Cdh1.

RESULTS

The NTD of Cdh1 is sufficient for cell cycle–regulated nuclear localization

Phosphorylation by Cdk1 prevents Cdh1 from binding to the APC/C core (Zachariae, Schwab, *et al.*, 1998). In addition, phosphorylated Cdh1 was found to translocate from the nucleus to the cytoplasm in budding yeast (Jaquenoud *et al.*, 2002). We sought to study the effects of phosphorylation in more detail and first focused on the subcellular localization of the APC/C activator. To identify localization elements in Cdh1, we created a series of GFP fusion constructs containing truncated or mutated Cdh1 derivatives and used spinning-disk confocal microscopy to analyze their subcellular localization in living yeast cells. Expression levels of the fusion constructs were also compared by Western analysis (Supplemental Figure S1). Cdh1 consists of a regulatory NTD, which harbors nine of its 11 consensus sites for Cdk1 phosphorylation, and a C-terminal domain (CTD), which carries the characteristic WD40 propeller involved in substrate binding (Figure 1A). In a first step, we fused either the NTD or CTD of Cdh1 to GFP, producing Cdh1(1-257)-GFP and GFP-Cdh1(245-566) constructs, expressed them from the constitutive *TEF2* promoter, and compared their localization with the cellular distribution of GFP-Cdh1, an N-terminal GFP fusion protein of full-length Cdh1, which was expressed transiently from the *MET25* promoter due to its potent inhibitory effect on cell division (Supplemental Figure S1B).

We found that the full-length Cdh1 construct, GFP-Cdh1, localized to the nucleus and the bud neck in a cell cycle–dependent manner, consistent with previous reports (Jaquenoud *et al.*, 2002; Martinez, Jeong, *et al.*, 2006). In unbudded, G1-phase cells and late-anaphase cells, GFP-Cdh1 resided in the nucleus, as judged by colocalization with a nuclear Cherry marker (Figure 1B, 1 and 4). In budded cells featuring a single nucleus, however, GFP-Cdh1 was detectable in the cytoplasm and showed only a weak nuclear staining (Figure 1B2). In addition to the cytoplasmic signal, GFP-Cdh1 was visible at the bud neck in budded cells (Figure 1B, 2 and 3), and colocalized with the septin Cdc11, which we visualized by integrating three copies of the mCherry-encoding gene at the 3′ end of endogenous *CDC11* (*CDC11-3mCherry*, Figure 1B5).

Of interest, the NTD of Cdh1 was sufficient to recapitulate the regulated nuclear localization of full-length Cdh1 (Figure 1C), as Cdh1(1-257)-GFP showed an intense nuclear signal in late mitotic and G1 phase cells (Figure 1C, 1 and 4) but little nuclear staining at other cell cycle stages (Figure 1C, 2 and 3). Unlike full-length Cdh1, Cdh1(1-257)-GFP failed to localize to the bud neck, consistent with the notion of a WD40 domain–mediated association with this compartment (Jaquenoud *et al.*, 2002; Martinez *et al.*, 2012). Indeed, the CTD construct GFP-Cdh1(245-566), which carries the WD40 domain, localized to the bud neck in budded cells (Figure 1D, 2 and 3). In addition, GFP-Cdh1(245-566) spread over the cytoplasm and was slightly enriched within the nucleus. In contrast to the NTD fusion Cdh1(1-257)-GFP, however, the distribution of GFP-Cdh1(245-566) between cytoplasm and nucleus remained constant during the cell cycle, indicating that the CTD of Cdh1 lacks sequences for regulated nuclear localization. Given that the WD40 domain functions in substrate recognition (Kraft *et al.*, 2005; Chao, Kulkarni, *et al.*, 2012; Tian, Li, *et al.*, 2012; He, Chao, *et al.*, 2013), localization of GFP-Cdh1(245-566) to the cytoplasm and nucleus might result from interactions with Cdh1 substrates. Taken together, these data show

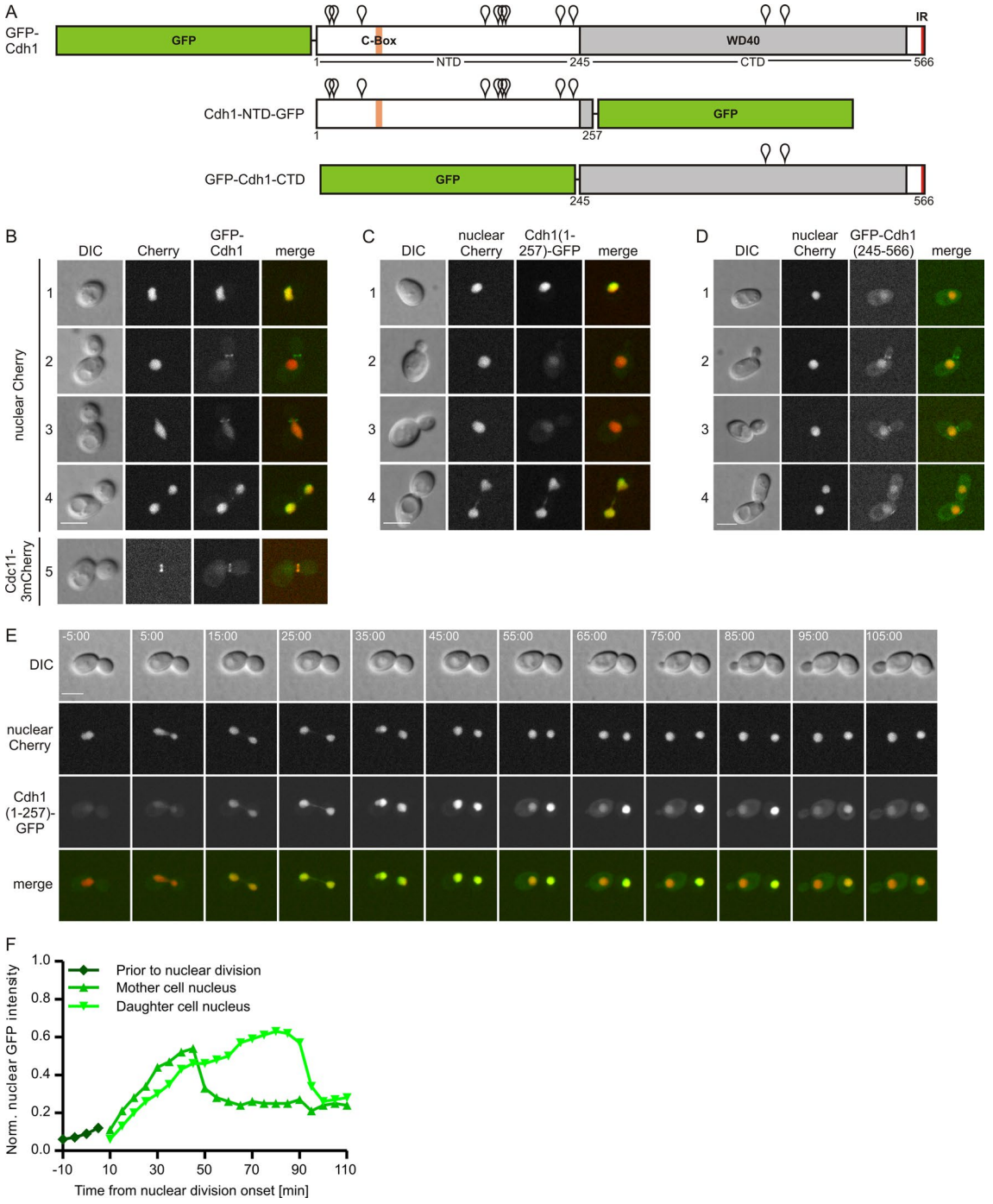

FIGURE 1: The NTD of Cdh1 is sufficient for cell cycle–regulated localization to the nucleus. (A) Schematic representation of GFP-Cdh1 fusion constructs. Positions of Cdk sites are indicated by white pins. The C-box (orange), the WD40 domain (gray), and the IR motif (red) are highlighted by colored boxes. Numbers indicate amino acid positions. NTD, N-terminal domain. CTD, C-terminal domain. (B) Live-cell imaging of cycling cells expressing *GFP-CDH1*. The construct was transiently expressed from the *MET25* promoter. Cells coexpressed either a nuclear Cherry marker or *CDC11-3mCherry* to visualize the nucleus or the septin ring, respectively. Representative cells (≥90%, $n > 100$) for different cell cycle stages. In the *CDC11-3mCherry* coexpressing strain (bottom), bud neck signals of GFP-Cdh1 and Cdc11-3mCherry were observed in 33 and 67% of the cells ($n = 128$), respectively. (C–F) Live-cell imaging of cycling cells expressing Cdh1(1-257)-GFP (C, E, and F) or GFP-Cdh1(245-566) (D) from the constitutive *TEF2* promoter. Cells coexpressed a nuclear Cherry marker to visualize the nucleus. (C, D) Representative cells (90%, $n > 100$) for different cell cycle stages. A bud neck signal of GFP-Cdh1(245-566) was observed in 60% of the cells ($n = 111$). (E) Time-lapse microscopy of Cdh1(1-257)-GFP with images taken at 5-min intervals. See Supplemental Movie S1E for full data. Shown are 10-min interval images for a representative cell. Elongation of the nucleus was defined as onset of nuclear division and used as time reference ($t = 0$ min). (F) Nuclear GFP intensities were measured for the cell shown in E, normalized to the maximum value of the total GFP intensity of both mother and daughter cell, and plotted against the time. DIC, differential interference contrast. Merge, merged GFP and Cherry images. Scale bar, 5 μm.

that the NTD of Cdh1 mediates regulated localization to the nucleus, whereas the CTD containing the WD40 domain is both required and sufficient for recruitment of Cdh1 to the bud neck.

Unlike full-length Cdh1, constitutive overexpression of the NTD construct Cdh1(1-257)-GFP produced a robust signal in microscopy without affecting cell growth (Supplemental Figure S1). This rendered Cdh1(1-257)-GFP a suitable construct to temporally resolve the regulated nuclear localization of Cdh1 by time-lapse microscopy. To this end, we imaged cells expressing Cdh1(1-257)-GFP at 5-min intervals for a period of 2 h to follow the protein through a complete cell division cycle (Figure 1E and Supplemental Movie S1E). We also measured the fluorescence intensities of nuclear GFP signals to quantitatively assess the changes in Cdh1(1-257)-GFP levels within the nucleus (Figure 1F). In budded cells, Cdh1(1-257)-GFP was distributed throughout the cell and slightly enriched in the nucleus. During nuclear division, the GFP signal in the nucleus gradually increased and, at the same time, decreased in the cytoplasm, indicating that Cdh1(1-257)-GFP was imported into the nucleus during anaphase. In late mitosis, Cdh1(1-257)-GFP localized to the nuclei of mother and daughter cells, and the corresponding signals reached maximal intensities. About 20 min after the completion of nuclear division, the nuclear GFP signal abruptly declined in the mother cell by >40% within 5 min. At the same time, a Cdh1(1-257)-GFP signal emerged in the cytoplasm, demonstrating that the fusion protein was exported to the cytoplasm. Of interest, nuclear export of Cdh1(1-257)-GFP was delayed in the respective daughter cell, in which nuclear levels of Cdh1(1-257)-GFP increased over a longer period and, depending on the length of the G1 phase, reached a plateau before nuclear export (Figure 1, E and F). This time lag was highly variable in individual cells, which argued that nuclear export of Cdh1(1-257)-GFP occurs independently in mother and daughter cells and is not closely linked to earlier mitotic events, such as spindle breakdown or cytokinesis. Instead, we found that export of Cdh1(1-257)-GFP to the cytoplasm strongly correlated with budding, which marks entry into a new cell cycle.

A similar localization pattern was observed in time-lapse analysis of the full-length GFP-Cdh1 construct. Owing to negative effects on cell growth (Supplemental Figure S1B), expression of GFP-Cdh1 had to be restricted to a low level. Like the NTD construct, GFP-Cdh1 accumulated in the nucleus during anaphase and reached a peak value in G1, and its nuclear levels decreased again when cells entered a new division cycle. For both constructs, about fivefold changes in nuclear levels were observed (Supplemental Figure S2). The partitioning between cytoplasm and nucleus could be more pronounced for endogenous Cdh1, which is expressed at a very low level (Kulak *et al.*, 2014).

The NTD of Cdh1 contains a regulated nuclear localization sequence

To narrow the region responsible for regulated nuclear localization of Cdh1, we fused truncations of the NTD to GFP and compared the subcellular localization of these constructs with Cdh1(1-257)-GFP (Figure 2A). We first cut the N-terminal domain into halves, which generated the constructs Cdh1(1-144)-GFP and Cdh1(145-257)-GFP. The latter construct, comprising the C-terminal portion of the NTD, Cdh1(145-257)-GFP, did not enrich in the nuclei of late mitotic cells (Figure 2A3). Instead, Cdh1(145-257)-GFP spread over the cell at all cell cycle stages in a pattern similar to nonfused GFP (Figure 2A1). Thus sequences within amino acids 145–257 of Cdh1 do not support nuclear localization.

In contrast to Cdh1(145-257)-GFP, the construct containing the N-terminal half of the Cdh1 NTD still showed regulated localization to the nucleus, as Cdh1(1-144)-GFP was predominantly cytoplasmic in preanaphase cells but nuclear in late mitotic cells (Figure 2A4 and Supplemental Movie S2A4). To compare the nuclear transport dynamics of Cdh1(1-144)-GFP to the original NTD construct, Cdh1(1-257)-GFP, we followed both fusion proteins by time-lapse microscopy and measured the increase and decrease of nuclear GFP signals in single cells over time. We used the onset of nuclear division and the emergence of a new bud as time reference points to align the resulting quantification curves obtained for nuclear import and nuclear export, respectively. We found that import of Cdh1(1-257)-GFP into the nucleus started 2.3 min (±5.3 min, 13 cells; Figure 2B) after onset of nuclear division. Nuclear levels of the fusion protein gradually increased more than fourfold on average (Figure 2B). Nuclear import of Cdh1(1-144)-GFP largely resembled that of the original NTD construct, as Cdh1(1-144)-GFP started to accumulate in the nucleus simultaneously (2.3 ± 3.3 min, 13 cells; Figure 2B) and with comparable dynamics. On comparing nuclear export of Cdh1(1-257)-GFP for individual cells, we found that the average time between first appearance of the fusion protein in the cytoplasm and discernible emergence of a new bud was 5.4 min (±3.2 min, 13 cells; Figure 2C) and did not differ between mother and daughter cells. Nuclear levels of Cdh1(1-257)-GFP declined rapidly within the first 15 min of export, which led to a reduction by ~50%, and decreased at slow rates thereafter (Figure 2C). Cdh1(1-144)-GFP was exported at the same time as Cdh1(1-257)-GFP, as its nuclear signal decreased 5.4 min (±3.8 min, 13 cells) before bud emergence. However, nuclear export of Cdh1(1-144)-GFP was somewhat reduced in such a way that nuclear levels of Cdh1(1-144)-GFP declined less rapidly than those of Cdh1(1-257)-GFP (Figure 2C).

The negative effect on nuclear export became even more pronounced when the C-terminal truncation was extended to produce Cdh1(1-100)-GFP (Figure 2A5 and Supplemental Movie S2A5). Although export started on time, Cdh1(1-100)-GFP was exported from the nucleus at very slow rates, so that its nuclear level remained >80% at 20 min after export onset (Figure 2C). Thus sequences within amino acids 101–257 contribute to efficient nuclear export of Cdh1. Unlike its deficiency in nuclear export, Cdh1(1-100)-GFP remained largely proficient for regulated import into the nucleus. Relative to Cdh1(1-144)-GFP or Cdh1(1-257)-GFP, Cdh1(1-100)-GFP was present in the nucleus at an elevated level before nuclear division (Figure 2, A and B), which likely arose from its inefficient export. Nevertheless, nuclear levels of Cdh1(1-100)-GFP considerably increased during anaphase (Figure 2, A5 and B), arguing that the N-terminal 100 residues of Cdh1 may harbor a cell cycle–regulated nuclear localization sequence (NLS), which becomes active during anaphase.

Indeed, bioinformatic analysis (Kosugi *et al.*, 2009) predicted a bipartite NLS within the NTD of Cdh1 at residues 24–50 (Figure 3A). To test the NLS prediction, we substituted basic residues of the putative NLS by alanines and analyzed the subcellular localization of the resulting Cdh1(1-257)-NLSm-GFP constructs. We observed a pronounced signal in the cytoplasm in anaphase cells in case of the NLSm1 construct lacking the four basic residues of the N-terminal stretch (Figure 3B1). Some mislocalization to the cytoplasm was also associated with mutating the three arginine residues of the C-terminal stretch (Figure 3B2). Combining these mutations in the NLSm1,2 construct essentially prevented nuclear enrichment (Figure 3B3). These data confirm the existence of a bipartite NLS element at residues 24–50 of Cdh1. Further C-terminal sequences may be needed for NLS function, since nuclear localization of the Cdh1(1-63)-GFP construct was compromised (Figure 2A6).

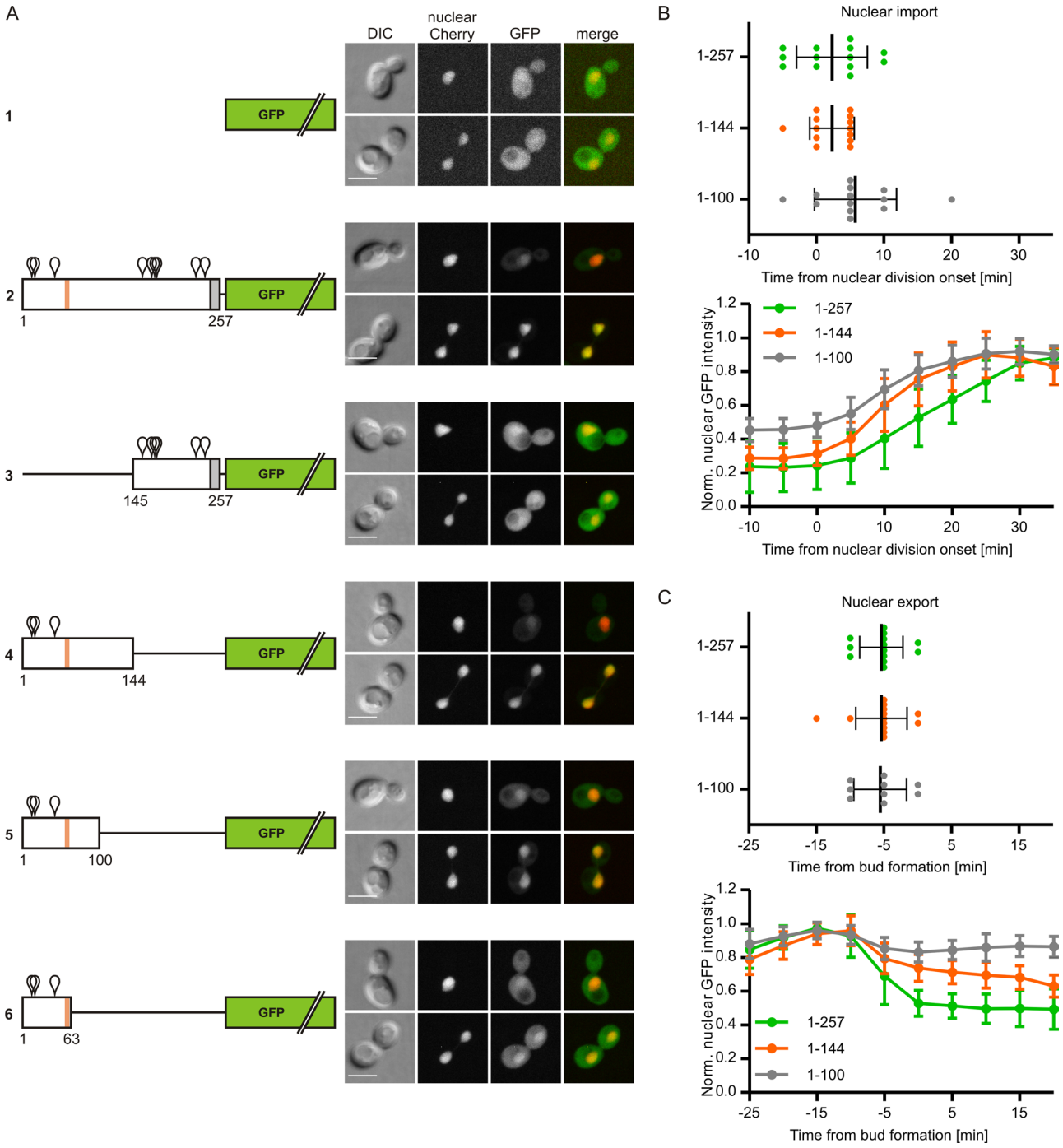

FIGURE 2: Regions within the NTD of Cdh1 relevant to nuclear transport. (A) Live-cell imaging of cycling cells expressing GFP fusions of the indicated *CDH1* truncation constructs or nonfused GFP from the constitutive *TEF2* promoter. For each construct, representative cells (≥90%, $n > 100$) of preanaphase (top) and late anaphase (bottom) are shown. Strains coexpressed a nuclear Cherry marker to visualize the nucleus. Left, diagrams of the constructs. Positions of Cdk sites are indicated by white pins, and deleted regions are illustrated by black lines. Cdh1 portions are drawn to scale, unlike GFP. Numbers indicate amino acid positions. Merge, merged GFP and Cherry images. Scale bar, 5 μm. (B, C) Comparison of Cdh1 truncation constructs for the timing and dynamics of their nuclear import (B) and export (C). Cycling cells expressing *CDH1(1-257)-GFP* (1–257, green), *CDH1(1-144)-GFP* (1–144, orange), or *CDH1(1-100)-GFP* (1–100, gray) were imaged at 5-min intervals, and fluorescence intensities of nuclear GFP signals were measured for individual cells. Top, time point at which the nuclear GFP intensity increased (B) or decreased (C) >10% defined as import start (B) or export start (C), respectively, and plotted vs. time. Each dot represents a single cell, and middle and error bars indicate the mean ± SD for each strain. Bottom, nuclear GFP intensities were measured and normalized to the individual maximum value. For each strain, mean ± SD for all cells is plotted vs. time. Elongation of the nucleus was defined as onset of nuclear division and used as time reference ($t = 0$ min) in B. The first visible change in cell shape at the future budding site was defined as onset of bud formation and used as time reference ($t = 0$ min) in C. Sample size is 13 for all strains, except for analysis of export timing for Cdh1(1-100)-GFP (dot plot in C), where nine cells were analyzed.

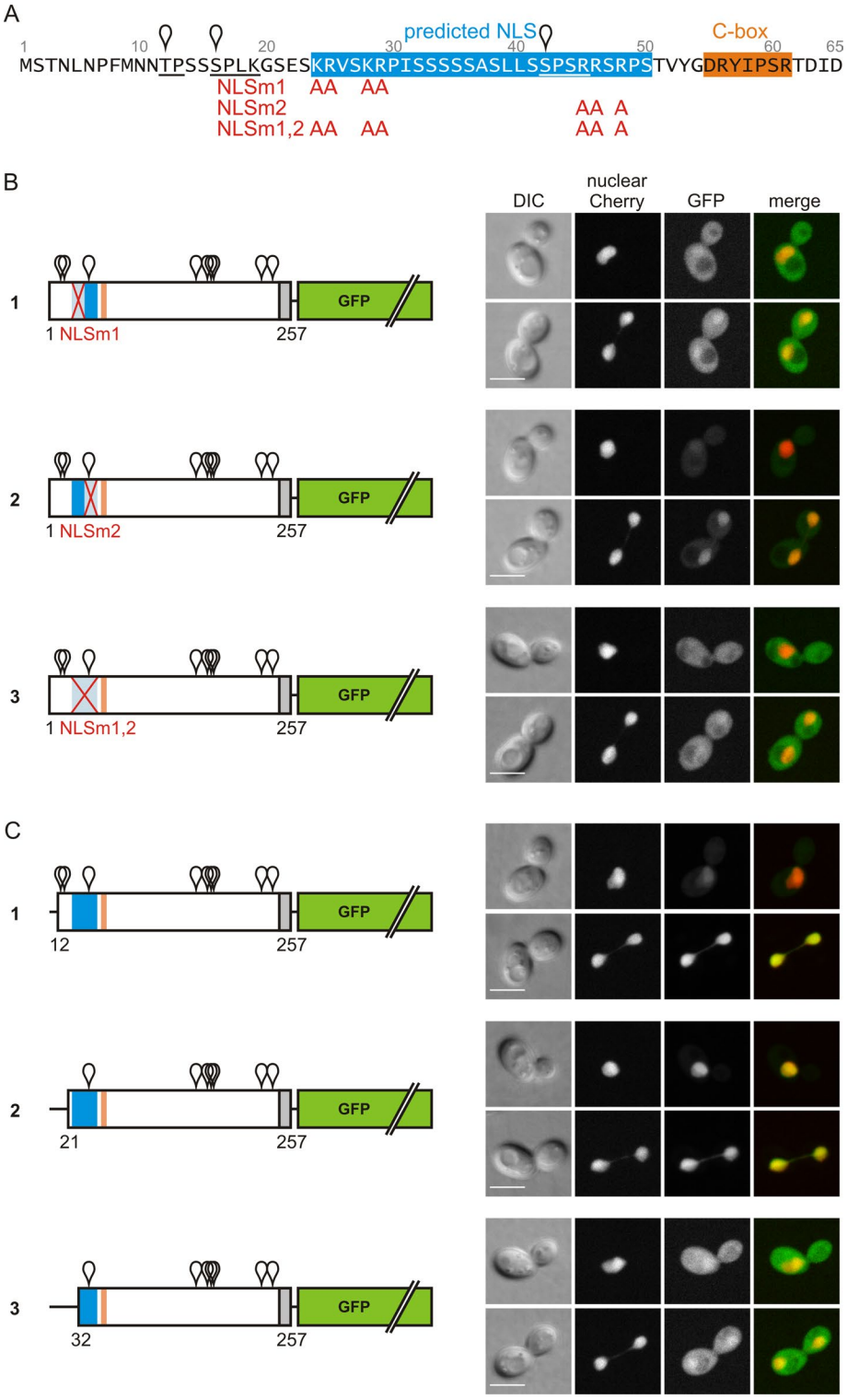

FIGURE 3: Sequences of the Cdh1-NTD needed for nuclear transport and its regulation. (A) Amino acid sequence of the N-terminal 65 residues of yeast Cdh1. Colored boxes highlight the C-box sequence (orange) and a bipartite NLS predicted by bioinformatic analysis (Kosugi *et al.*, 2009) within residues 24–50 (blue). Mutations of the predicted NLS by alanine substitutions (NLSm1, NLSm2, and NLSm1,2) are shown by red A below the mutated residues. The positions of Cdk sites are indicated by white pins, and their sequence is underlined. Numbers indicate amino acid positions. (B, C) Live-cell imaging of cycling cells expressing GFP fusions of the indicated *CDH1* mutant (B) or truncation constructs (C) from the constitutive *TEF2* promoter. For each construct, representative cells (≥90%, $n > 100$) of preanaphase (top) and late anaphase (bottom) are shown. Strains coexpressed a nuclear Cherry marker to visualize the nucleus. Left, diagrams of the Cdh1-GFP constructs. Positions of Cdk sites are indicated by white pins. Mutations of the predicted NLS (NLSm1, NLSm2, and NLSm1,2; see above) are labeled by a red cross, and deleted regions are indicated by black lines. The Cdh1 portions are drawn to scale, unlike GFP. Numbers indicate amino acid positions. Merge, merged GFP and Cherry images. Scale bar, 5 μm.

Of interest, the identified NLS element is preceded by two Cdk sites and overlaps with another one (Figure 3A). Because Cdk1 phosphorylation has been described to control NLS activity in several cases (Moll *et al.*, 1991; Sidorova *et al.*, 1995; O'Conallain *et al.*, 1999; Liku *et al.*, 2005; Kosugi *et al.*, 2009), we wondered whether this might also apply to the NLS of Cdh1. As a first approach, we generated N-terminal truncation constructs. Cdh1(12-257)-GFP, which lacks residues 1–11 of Cdh1, resembled the full-length NTD construct in showing a cytoplasmic and weak nuclear signal before anaphase but an intense nuclear signal in late anaphase (Figure 3C1). Thus the N-terminal 11 residues of Cdh1 are dispensable for regulated nuclear localization. In contrast, Cdh1(21-257)-GFP, which lacks the first two Cdk sites but retains the predicted NLS intact, was nuclear not only in late mitosis but also before anaphase (Figure 3C2). This largely constitutive localization to the nucleus pointed to a critical role of Cdk sites 1 and 2 in controlling nuclear translocation of Cdh1. Further truncation of this construct, which eliminated the N-terminal basic stretch of the predicted bipartite NLS, interfered with nuclear import of the protein. Like the NLSm1 mutant, the resulting Cdh1(32-257)-GFP was mostly cytoplasmic and failed to accumulate in the nucleus during anaphase (Figure 3C3). These data confirm the predicted NLS and show that its N-terminal basic stretch is required for proper nuclear localization. The data indicate, moreover, that the region preceding the NLS, which contains Cdk sites 1 and 2, is critical for the cell cycle–dependent nuclear localization of Cdh1.

Cdk phosphorylation sites 1–3 regulate nuclear localization of Cdh1

To study more deeply how nuclear import of Cdh1 is controlled by Cdk1 phosphorylation, we replaced the serine or threonine residues of all nine Cdk sites within the NTD of Cdh1 by alanine to create a nonphosphorylatable version named Cdh1(1-257)-m(1-9)A-GFP. Time-lapse microscopy revealed that this phosphosite mutant version, unlike wild-type Cdh1(1-257)-GFP, no longer shuttled between the cytoplasm and the

nucleus (Figure 4A and Supplemental Movie S4A). Instead, Cdh1(1-257)-m(1-9)A-GFP localized to the nucleus at all cell cycle stages, and its nuclear levels remained constant throughout the cell cycle (Figure 4A). This indicates that nuclear localization of Cdh1 is prevented by phosphorylation of Cdk sites within the NTD.

The finding that Cdh1(1-144)-GFP, which retains only Cdk sites 1–3, still localized to the nucleus in a cell cycle–regulated manner (Figure 2) suggested that Cdk sites 4–9 might be dispensable for the control of Cdh1 localization. To test this idea, we eliminated Cdk sites 4–9 in Cdh1(1-257)-GFP by replacing the respective serine or threonine residues by alanines while leaving the other Cdk sites unchanged. In addition, we created a complementary construct in which Cdk sites 1–3 were mutated and Cdk sites 4–9 were left intact. The m(4-9)A mutant, in which phosphorylation at Cdk sites 1–3 is still possible, accumulated in the nucleus during anaphase and relocalized to the cytoplasm at the end of G1 phase (Figure 4B and Supplemental Movie S4B). Moreover, quantification of nuclear GFP levels revealed that nuclear import and export of the m(4-9)A mutant occurred with kinetics very similar to that of the wild-type NTD construct Cdh1(1-257)-GFP (Figure 4, D and E). These results indicate that Cdk sites 1–3 are sufficient to control Cdh1 localization to the nucleus. Consistent with this conclusion, mutation of Cdk sites 1–3 alone disrupted the nucleocytoplasmic shuttling of Cdh1(1-257)-GFP. Like the m(1-9)A construct lacking all Cdk sites, the m(1-3)A mutant resided in the nucleus, and its nuclear levels remained constant during the cell cycle (Figure 4C and Supplemental Movie S4C). Taken together, these data argue that nuclear localization of Cdh1 during the cell division cycle is controlled by phosphorylation at Cdk sites 1–3.

Cdk phosphorylation sites 4–9 control Cdh1 binding to the APC/C

Recent work indicates that APC/C-Cdh1 activity is restricted to the nucleus in budding yeast (Arnold, Höckner, *et al.*, 2015). Therefore nuclear localization of Cdh1 is expected to be a prerequisite for its biological function. Cdk sites 4–9 of Cdh1 were not involved in the control of nuclear localization (Figures 2 and 4), yet an earlier study showed that their removal increased the in vivo activity of Cdh1 (Zachariae, Schwab, *et al.*, 1998), indicating an important regulatory role. To define further the significance of these phosphorylation sites, we introduced various combinations of Cdk site mutations into full-length Cdh1 (Figure 5A). For expression at comparable levels, single-copy chromosomal integrations were generated by use of a disintegrator vector system (Sadowski *et al.*, 2007). To test their ability to bind the APC/C in vivo, Cdh1 and its phosphosite mutants were immunoprecipitated by an N-terminal triple-hemagglutinin (HA3) epitope. Cells coexpressed a Myc9-tagged version of the APC/C subunit Cdc23 from its endogenous locus to assess the amounts of coprecipitated APC/C in Western analysis. In addition, we determined levels of the mitotic cyclin Clb2 in whole-cell extracts as an indicator for the competence of an overexpressed Cdh1 derivative to activate the APC/C and thereby trigger Clb2 degradation.

Because subcellular compartments are disrupted during the preparation of whole-cell protein extracts, we checked beforehand whether coprecipitation would specifically recover APC/C-Cdh1 complexes present in living cells before cell lysis as opposed to complexes of cytoplasmic Cdh1 with nuclear APC/C that might form de novo in cell extracts after cell disruption. To this end, we expressed Cdc23-Myc9 and HA3-Cdh1 separately in haploid strains and mixed them before cell lysis. For comparison, we coexpressed Cdc23-Myc9 and HA3-Cdh1 in a heterozygote diploid strain. Whereas Cdc23-Myc9 was present in immunoprecipitates of HA3-Cdh1 prepared from extracts of the coexpressing diploid strain, only background levels of Cdc23-Myc9 were detected in HA3-Cdh1 precipitates from the mixed haploid strains (Supplemental Figure S3A). Thus postlysis formation of APC/C-Cdh1 complexes is negligible in this analysis. Moreover, Cdc23-Myc9 failed to coprecipitate with a version of HA3-Cdh1 whose nuclear localization sequence was inactivated by the NLSm1,2 mutation (Supplemental Figure S3B), further supporting the view that coprecipitation recovered complexes of Cdh1 formed with the APC/C in vivo.

In a first step, we studied APC/C binding in cells arrested in mitosis by treatment with the spindle poison nocodazole. In these cells, Cdk1 activity, and thus Cdh1 phosphorylation, is maximal. As revealed by fluorescence microscopy of cells expressing *CDH1* fused to GFP, wild-type Cdh1 localized to the cytoplasm and failed to enrich in the nucleus of nocodazole-treated cells (Figure 5B, top). In contrast, a GFP-tagged version of the APC/C subunit Cdc23 was nuclear under these conditions (Supplemental Figure S4A). Consistent with being phosphorylated at multiple positions, HA3-Cdh1 migrated heterogeneously in SDS–PAGE and largely failed to bind the APC/C, since immunoprecipitates of HA3-Cdh1 contained little, if any, Cdc23-Myc9 above the background level (Figure 5C, lane 9). Furthermore, overexpressed HA3-Cdh1 failed to reduce Clb2 levels in cell extracts (Figure 5C, lane 2). These data indicate that wild-type Cdh1 is phosphorylated, cytoplasmic, and unable to bind or activate the APC/C in nocodazole-arrested cells.

To examine how the localization of Cdh1 influences its interaction with the APC/C, we introduced the m(1-3)A mutation into full-length Cdh1 to provoke constitutive nuclear localization. As expected, inactivation of Cdk sites 1–3 caused GFP-Cdh1 to localize to the nucleus in the majority of the nocodazole-arrested cells (Figure 5B, middle). Despite the enhanced nuclear localization, the m(1-3)A mutation hardly improved coprecipitation of Cdc23-Myc9 with HA3-Cdh1 (Figure 5C, lanes 9 and 10). Thus nuclear localization of Cdh1 is per se not sufficient for robust binding of the activator to the APC/C core, suggesting that APC/C binding of the nuclear Cdh1-m(1-3)A might be inhibited by the remaining Cdk sites in the NTD of Cdh1. These sites are organized into two clusters: Cdk sites 4–7 within residues 157–177 and Cdk sites 8 and 9 at residues 227 and 240 near the end of the NTD of Cdh1 (Figure 5A). Indeed, the APC/C interaction of Cdh1-m(1-3)A was enhanced when we eliminated either Cdk sites 4–7 or Cdk sites 8 and 9 in this construct. The resulting m(1-7)A and m(1-3, 8-9)A mutants both bound considerably more Cdc23-Myc9 than Cdh1-m(1-3)A in the coprecipitation analysis (Figure 5C, lanes 10, 12, and 13), indicating that phosphorylation at both Cdk site clusters, 4–7 and 8 and 9, might inhibit APC/C binding of Cdh1. Moreover, we observed maximal APC/C binding when we mutated all nine Cdk sites within the Cdh1 NTD (Figure 5C, lane 14), indicating that the effects of Cdk sites 4–7 and Cdk sites 8 and 9 on the APC/C-Cdh1 interaction are additive. Furthermore, we found that mutating Cdk sites 4–9 of Cdh1 improved the interaction with the ubiquitin ligase only when Cdk sites 1–3 were mutated as well, as the m(4-9)A mutant bound substantially less Cdc23-Myc9 than the m(1-9)A mutant (Figure 5C, lanes 11 and 14). Because the m(4-9)A mutant, which retains phosphorylation at Cdk sites 1–3, was cytoplasmic in most nocodazole-arrested cells (Figure 5B, bottom), we conclude that Cdh1 must reside in the nucleus to bind the APC/C.

Analysis of the levels of the mitotic cyclin Clb2 in cell extracts indicated that the ability of the Cdh1 constructs to stimulate Clb2 degradation mostly correlated with the degree of their APC/C binding (Figure 5C). Because Cdh1-m(1-3)A and Cdh1-m(4-9)A bound the APC/C only weakly but decreased Clb2 levels by >50%, small

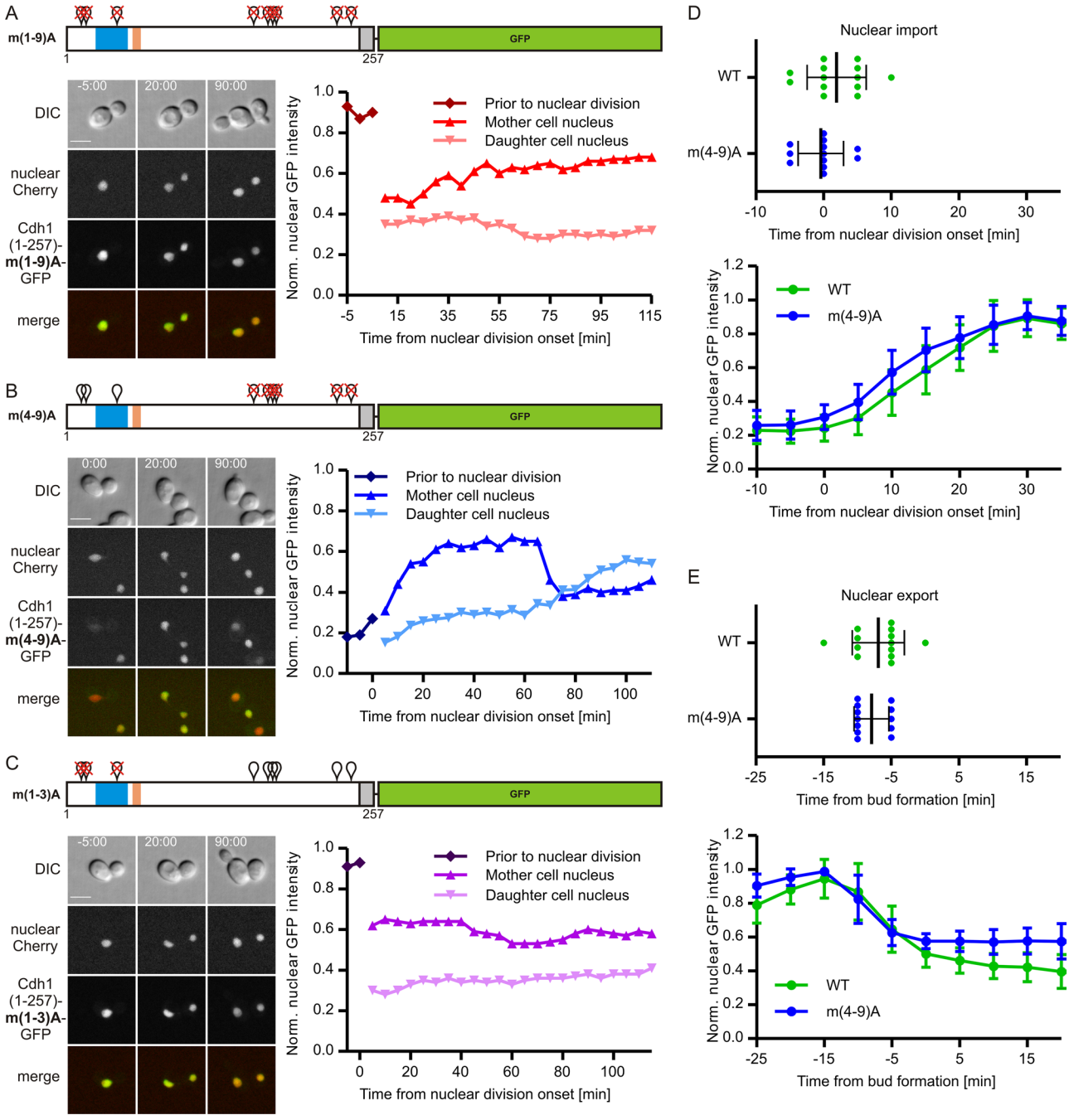

FIGURE 4: Cdk sites 1–3 control localization of Cdh1(1-257)-GFP to the nucleus. (A–E) Live-cell imaging of cycling cells expressing *CDH1(1-257)-m(1-9)A-GFP* (A), *CDH1(1-257)-m(4-9)A-GFP* (B, D, E), *CDH1(1-257)-m(1-3)A-GFP* (C), or *CDH1(1-257)-GFP* (D, E) from the constitutive *TEF2* promoter. Cells were imaged at 5-min intervals (see also Supplemental Movies S4A–S4C). (A–C) Left, selected time points of cells expressing the indicated mutant constructs. Right, nuclear GFP intensities of these cells were measured, normalized, and plotted against the time as in Figure 1F. Elongation of the nucleus was defined as onset of nuclear division and used as time reference ($t = 0$ min). Diagrams of the constructs are given above. Positions of Cdk sites are indicated by white pins, and mutation of their phosphoaccepting residues to alanines (S/TP changed to AP) are labeled by red crosses. The NLS (blue) and the C-box (orange) are highlighted by colored boxes. Merge, merged GFP and Cherry images. Scale bar, 5 μm. (D, E) Comparison of Cdh1(1-257)-GFP (WT, green) and Cdh1(1-257)-m(4-9)A-GFP (m(4-9)A, blue) for the timing and dynamics of their nuclear import (D) and export (E). Total fluorescence intensities of nuclear GFP signals were analyzed as in Figure 2, B and C. Top, each dot represents a single cell, and middle and error bars indicate mean ± SD for each strain. Bottom, mean ± SD for all cells of the respective strains. Sample sizes were 13 for Cdh1(1-257)-GFP and 12 for Cdh1(1-257)-m(4-9)A-GFP.

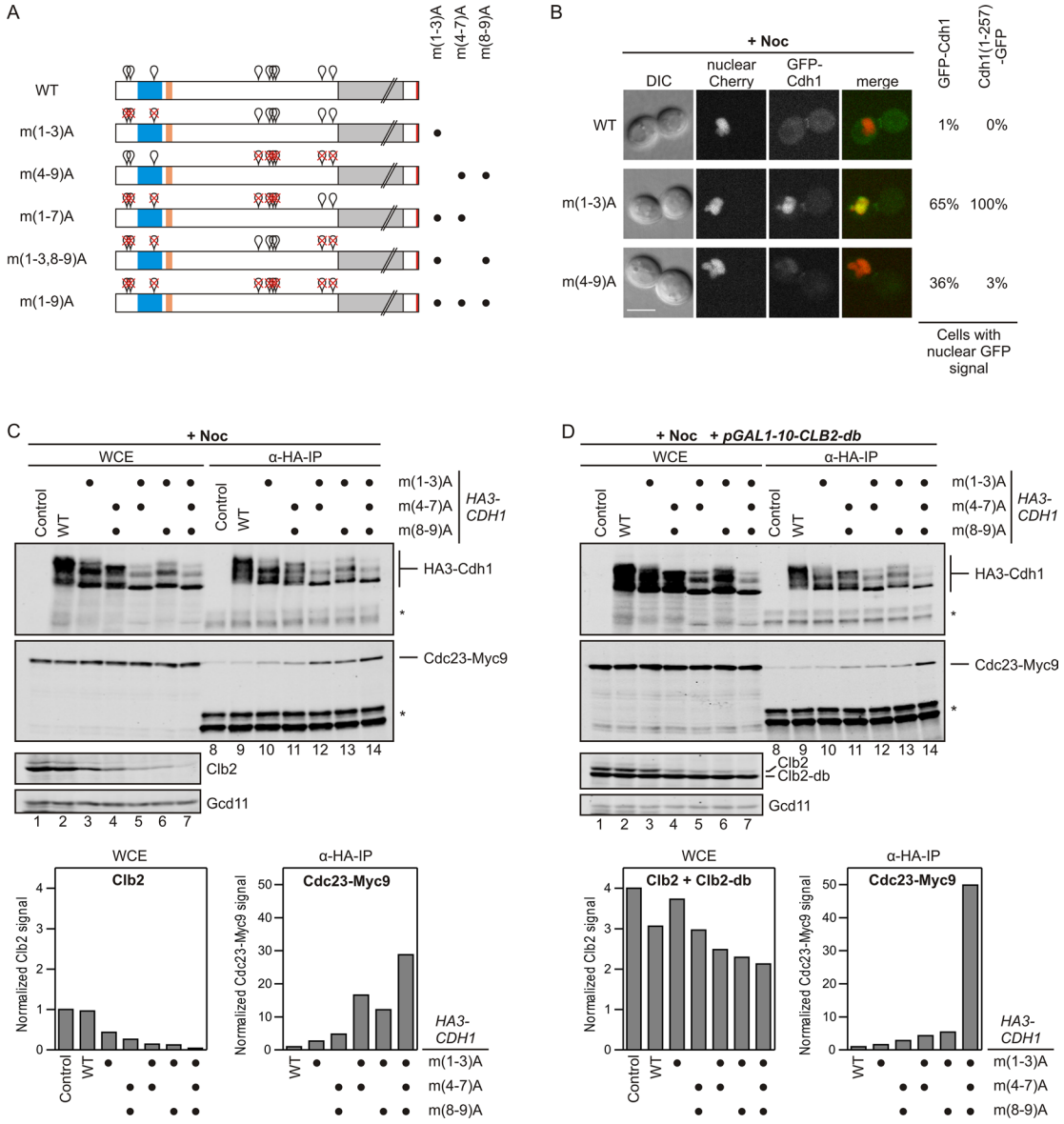

FIGURE 5: Cdk sites 4–9 control the binding of Cdh1 to the APC/C in mitotic cells. (A) Schematic representations of the Cdh1 derivatives. Positions of the NLS (blue), the C-box (orange), the WD40 domain (gray, not drawn to scale), the IR motif (red), and Cdk sites (white pins). Mutation of Cdk sites to alanines (S/TP to AP) is indicated by red crosses. (B) Live-cell imaging of nocodazole (Noc)-arrested cells expressing *GFP-CDH1*, *GFP-CDH1-m(1-3)A*, or *GFP-CDH1-m(4-9)A* from the *MET25* promoter. Cdh1 constructs were expressed for 45 min in cells pretreated with Noc for 3 h. Strains carried a nuclear Cherry marker to visualize the nucleus. Representative cells are shown. Right, fraction of cells showing a nuclear GFP signal (sample size was 87 for GFP-Cdh1, 43 for m(1-3)A, and 39 for m(4-9)A). The quantified nuclear localization of equivalent Cdh1(1-257)-GFP versions is indicated for comparison (sample size was 63 for Cdh1(1-257)-GFP, 42 for m(1-3)A, and 70 for m(4-9)A). Cells expressing these *CDH1(1-257)-GFP* versions are shown in Supplemental Figure S4. Merge, merged GFP and Cherry images. Scale bar, 5 μm. (C) APC/C binding of HA3-Cdh1 (WT) and the indicated phosphosite mutants in Noc-arrested cells. Various constructs of *HA3-CDH1* were expressed from the *GALL* promoter for 2 h in cells pretreated with Noc for 3 h. HA3-Cdh1 and its phosphosite mutants were immunoprecipitated with HA-specific antibody. Whole-cell extracts (WCEs) and immunoprecipitates (α-HA-IP) were analyzed by Western blotting with HA- and Myc-specific antibodies to detect precipitated Cdh1 proteins and coprecipitated Cdc23-Myc9 expressed from its endogenous gene locus. A *CDC23-MYC9* strain lacking the *HA3-CDH1* construct served as control (lanes 1 and 8). WCEs were also probed for endogenous levels of Clb2 and Gcd11, which served as loading control, in a separate Western blot analysis using indicated antisera. Histograms show quantifications of Clb2 signals in WCEs (left) and Cdc23-Myc9 signals in immunoprecipitates (right). Clb2 signal intensities were normalized to the corresponding Gcd11 signals, with the value for the *CDC23-MYC9* control strain set to 1. Signal intensities of coprecipitated Cdc23-Myc9 were measured, adjusted for Cdh1 recovery, and then normalized to the value of wild-type Cdh1, which was set to 1. *Immunoglobulin G (IgG) bands. (D) APC/C binding of HA3-Cdh1 (WT) and the indicated phosphosite mutants in Noc-arrested cells overexpressing Clb2-db, a stabilized version of Clb2 lacking the destruction box motif (Schwab *et al.*, 1997). Nocodazole treatment, expression of Cdh1 derivatives and Clb2-db, immunoprecipitation, Western blotting, signal intensity measurements of total Clb2 (Clb2 + Clb2-db) and Cdc23-Myc9 levels, and normalization were performed as in C. *IgG bands.

amounts of Cdh1 bound to the APC/C appear to be sufficient to promote Clb2 degradation. Consistent with an increased APC/C activation capacity, the m(1-3)A and m(4-9)A constructs compromised cell growth even at low expression levels (Supplemental Figure S1B). Ectopic APC/C activation and a negative feedback on Cdk1 activity might explain why full-length constructs carrying these mutations localize less homogenously than the corresponding Cdh1(1-257) constructs (Figure 5B and Supplemental Figure S4B), which are unlikely to activate the APC/C toward B-type cyclins.

The observed reduction of Clb2 levels suggested that the phosphorylation of Cdk sites in a range of proteins, such as core subunits of the APC/C, was lowered by expression of various Cdh1 constructs. To ask whether reduced phosphorylation of proteins other than Cdh1 contributed to APC/C-Cdh1 binding, we repeated the coprecipitation experiment in cells that expressed Clb2-db, a stabilized version of Clb2 lacking the destruction box motif (Schwab *et al.*, 1997), to maintain mitotic levels of Cdk1 activity. As expected, Clb2-db did not respond to the expression of activated Cdh1 constructs and persisted at levels at least twofold above the regular mitotic level of Clb2 (Figure 5D). Under these conditions, the m(1-9)A mutant of Cdh1 efficiently associated with the APC/C, whereas the m(1-7)A and m(1-3)A-m(8-9)A constructs of Cdh1, which retained Cdk sites at positions 4–7 or 8 and 9, were reduced for APC/C interaction relative to the situation in which Clb2-db was not expressed (Figure 5, C and D, lanes 12–14). These data indicate that the phosphorylation of Cdk sites 4–7 or 8 and 9 is sufficient to prevent Cdh1 from binding to the APC/C and confirm the crucial role of Cdk phosphorylation sites in Cdh1 in controlling the formation of the APC/C-Cdh1 complex.

To further investigate the role of Cdk sites 4–9 of Cdh1, in a next step, we replaced the serine and threonine residues at these positions by aspartates to imitate constitutive phosphorylation and examined the APC/C-Cdh1 interaction in asynchronously growing, unperturbed cells. As indicated by coprecipitation of Cdc23-Myc9 with HA3-Cdh1, wild-type Cdh1 bound to the APC/C in extracts of cycling cells (Figure 6, lane 9), which contain a portion of unphosphorylated Cdh1 derived from cells in late mitosis and G1. The phosphomimetic version, Cdh1-m(4-9)D, however, failed to interact with the APC/C, whereas the mutant version that was nonphosphorylatable at these sites, Cdh1-m(4-9)A, bound to the APC/C more efficiently than the wild-type Cdh1 (Figure 6, lanes 8–11). The mutations of Cdk sites 4–9 caused essentially the same effect when introduced into the m(1-3)A version of Cdh1, which is localized to the nucleus constitutively. Cdc23-Myc9 coprecipitated with Cdh1-m(1-3)A, but only background levels were recovered with the m(1-3)A-m(4-9)D construct (Figure 6, lanes 12 and 13), whereas increased amounts of Cdc23-Myc9 relative to Cdh1-m(1-3)A coprecipitated with the Cdh1-m(1-9)A construct, which combines the m(1-3)A and m(4-9)A mutations (Figure 6, lanes 12 and 14). The m(4-9)D mutation affected neither the regulated nuclear localization of Cdh1(1-257)-GFP nor the constitutive nuclear localization of the Cdh1(1-257)-m(1-3)A construct (Supplemental Figure S5), indicating that protein mislocalization cannot be the cause of the observed APC/C binding defects of m(4-9)D mutants of Cdh1. We thus conclude that phosphorylation at Cdk sites 4–9 interferes with the binding of Cdh1 to the APC/C. The ability of overexpressed Cdh1-m(4-9)D mutants to reduce Clb2 levels (Figure 6, lanes 3 and 6) might stem from the failure of aspartate residues to fully imitate the phosphorylation of these Cdk sites.

Alanine replacements at Cdk sites 1–3 to allow for constitutive nuclear localization of Cdh1 did not increase the APC/C binding of Cdh1 (Figure 6, lanes 9 and 12) but did enhance the function of the

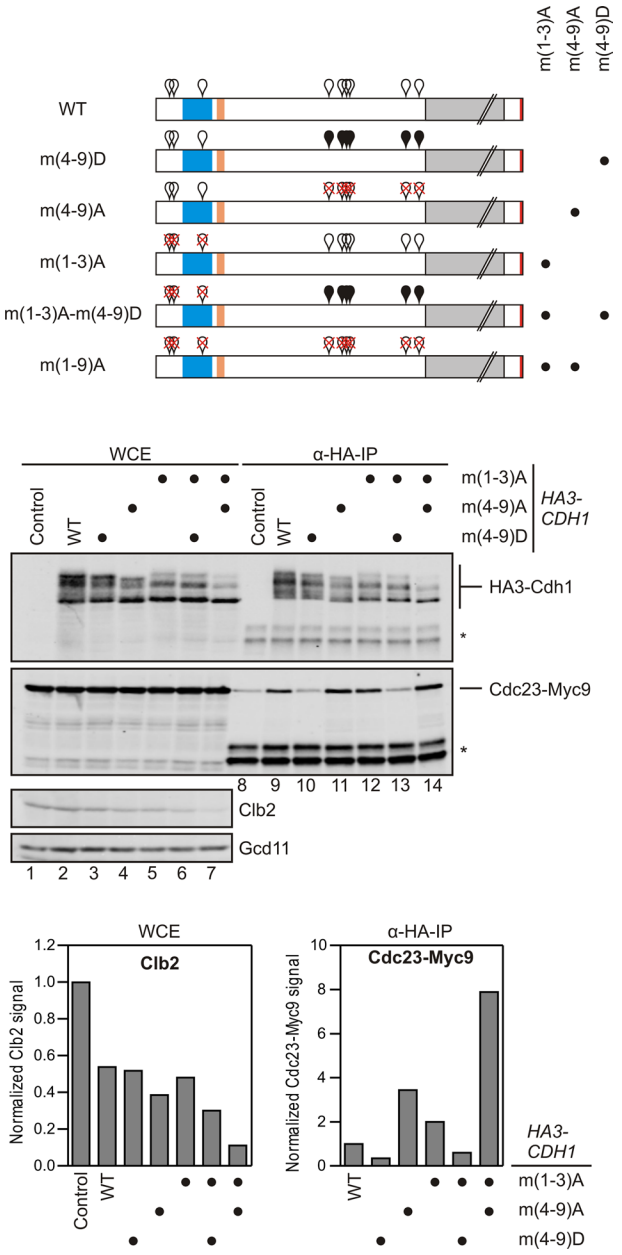

FIGURE 6: Cdk sites 4–9 control the binding of Cdh1 to the APC/C in nonsynchronized cells. Schematic representations of the Cdh1 derivatives. Positions of the NLS (blue), the C-box (orange), the WD40 domain (gray, not drawn to scale), the IR motif (red), and Cdk sites (white pins). Mutation of Cdk sites to alanines (S/TP to AP) are indicated by red crosses, and mutation of Cdk sites to aspartates (S/TP to DP) are indicated by black pins. APC/C binding of HA3-Cdh1 (WT) and the indicated phosphosite mutants was analyzed in nonarrested, cycling cells. Wild-type or mutant derivatives of *HA3-CDH1* were expressed from the *GALL* promoter for 2 h in cycling cells that coexpressed *CDC23-MYC9* from the endogenous gene locus. Immunoprecipitation, Western blotting, intensity measurements, and signal normalization were performed as in Figure 5C. *IgG bands.

Cdh1-m(4-9)A version, because the Cdh1-m(1-9)A mutant bound more Cdc23-Myc9 (Figure 6, lanes 11 and 14) and reduced Clb2 levels more severely than did the Cdh1-m(4-9)A mutant (Figure 6, lanes 4 and 7). These data confirm the view that nuclear localization is critical but not sufficient for Cdh1 function. Aspartate substitutions

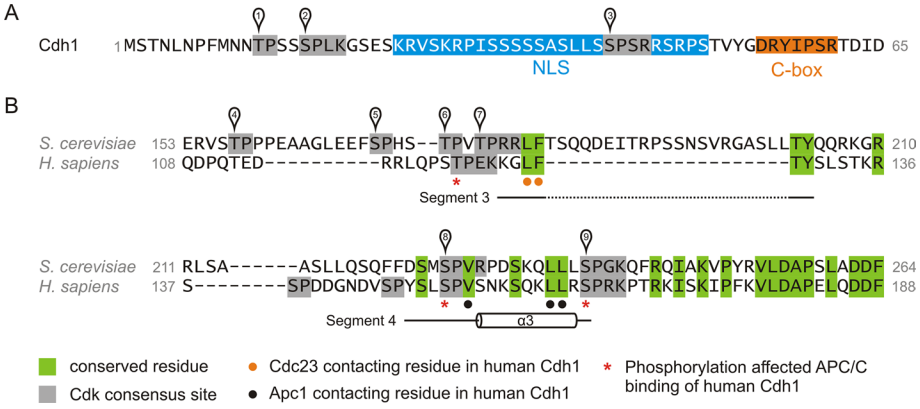

FIGURE 7: Separate Cdk sites control nuclear localization and APC/C binding of yeast Cdh1. (A) Amino acid sequence of the N-terminal 65 residues of Cdh1. Cdk consensus sites (gray), the NLS (blue), and the C-box (orange) are highlighted by color. Phosphorylated residues of Cdk sites are labeled by pins and numbered. (B) Sequence alignment of budding yeast and human Cdh1 orthologues showing APC/C-binding sites and adjacent Cdk sites. Identical residues (green) and Cdk consensus sites (gray) are highlighted in color. Phosphorylated residues of Cdk sites in budding yeast Cdh1 are labeled by pins and numbered. Orange and black dots indicate critical residues identified to contact Cdc23 and Apc1 in human APC/C, respectively (Chang, Zhang, *et al.*, 2015). Red asterisks indicate Cdk sites whose phosphorylation prevents APC/C binding of human Cdh1 (Chang, Zhang, *et al.*, 2015). Ordered regions are illustrated by lines and helices according to Chang, Zhang, *et al.* (2015).

at Cdk sites 1–3 were compatible with APC/C binding but affected the regulated nuclear localization of a Cdh1-NTD construct (Supplemental Figure S3, B and C). The differential behavior of the phosphomimetic m(1-3)D and m(4-9)D mutations supports the notion of separate functions associated with these Cdk sites of Cdh1.

Proteins with multiple Cdk sites may be phosphorylated in a cascade-like manner. In one such mechanism, the Cdk1 complex uses its phosphoadaptor subunit Cks1 to bind a Cdk docking site (Koivomägi *et al.*, 2011, 2013; McGrath, Balog, *et al.*, 2013). Because the Cdk site 7 of Cdh1 fits the consensus sequence for Cks1 binding, we analyzed the consequence of mutating site 7 alone. In mitotic cells, the m7A mutant of HA3-Cdh1 was still phosphorylated at multiple positions, as indicated by its heterogeneous mobility in SDS–PAGE, and resembled the wild-type version of HA3-Cdh1 in its inability to coprecipitate Cdc23-Myc9 under these conditions (Supplemental Figure S6, lanes 8 and 9). Moreover, in the nuclear-localized m(1-3)A version, coprecipitation of Cdc23-Myc9 increased when the m(4-6)A mutation was combined with m7A and increased further when m(8-9)A was added (Supplemental Figure S6, lanes 10–12). Thus there is no evidence for a critical role of the Cdk site 7 in priming phosphorylations at other Cdk sites of Cdh1.

DISCUSSION

The ubiquitin ligase APC/C-Cdh1 is restricted in its function to cell cycle stages of low Cdk activity, that is, late mitosis and G1, due to inactivation of the Cdh1 activator by phosphorylation at multiple Cdk sites (Zachariae, Schwab, *et al.*, 1998; Jaspersen *et al.*, 1999; Kramer *et al.*, 2000). Earlier work showed that all nine Cdk sites in the NTD of budding yeast Cdh1 contribute to inactivation (Zachariae, Schwab, *et al.*, 1998), but details of the underlying mechanism and the significance of having multiple phosphorylation sites remained unclear. This work reports that Cdk sites of budding yeast Cdh1 are organized into autonomous subgroups that control either the nuclear localization of Cdh1 or the binding of Cdh1 to the APC/C core complex. Thus the Cdk phosphorylation sites of yeast Cdh1 operate through distinct mechanisms. This sets Cdh1 apart from other target proteins of Cdk1, for which multisite phosphorylation events often synergize toward a single molecular outcome (Deshaies and Ferrell, 2001; Ferrell and Ha, 2014).

Unlike the APC/C core complex, which is constitutively nuclear localized in budding yeast cells (Zachariae, Shin, *et al.*, 1996; Melloy and Holloway, 2004), Cdh1 is cytoplasmic before mitosis, accumulates in the nucleus during anaphase, and relocates to the cytoplasm again in late G1 (Figure 1; Jaquenoud *et al.*, 2002). In this work, we identified a bipartite NLS near the N-terminal end of Cdh1 (Figure 3). Of interest, the function of this NLS was controlled by the phosphorylation of Cdk sites 1–3, since removal of sites 1 and 2 or alanine replacements at sites 1–3 to render them nonphosphorylatable resulted in constitutive nuclear localization (Figures 3 and 4C). Thus Cdh1 carries a Cdk-inhibited NLS, a localization control element common to various other proteins that shuttle between the nucleus and cytoplasm in a cell cycle–dependent manner (Moll *et al.*, 1991; Sidorova *et al.*, 1995; O'Conallain *et al.*, 1999; Liku *et al.*, 2005; Kosugi *et al.*, 2009). Within the NLS of Cdh1, Cdk site 3 resides at an optimal position for negative regulation of nuclear import (Figure 7; Kosugi *et al.*, 2008, 2009). The precise mechanism by which Cdk sites 1 and 2 control NLS function remains to be determined.

In addition to cell cycle–regulated import into the nucleus, our study provides evidence for nuclear export of Cdh1 at the end of G1 phase, as the decrease in nuclear levels of Cdh1(1-257)-GFP was accompanied by an increase of the signal in the cytoplasm (Figure 1E and Supplemental Movie S1E). Earlier work pointed to a role of the exportin Msn5 in nuclear export of Cdh1 and implicated N-terminal sequences of Cdh1 in Msn5 binding (Jaquenoud *et al.*, 2002). Our truncation analysis indicates that residues 101–257 of Cdh1 are needed for efficient export to the cytoplasm (Figure 2), suggesting that multiple sequence motifs might support Msn5 binding. Indeed, Msn5 interacting regions identified in other studies span 100 or more residues and do not share apparent similarities (DeVit and Johnston, 1999; Boustany and Cyert, 2002; Ueta *et al.*, 2007), impeding the determination of a consensus sequence for Msn5-mediated nuclear export, unlike the situation for the exportin Crm1 (Kutay and Guttinger, 2005). In several cases, phosphorylation of the exported proteins promoted their binding to Msn5, resulting in regulated nuclear export (Kaffman *et al.*, 1998; DeVit and Johnston, 1999; Boustany and Cyert, 2002; Ueta *et al.*, 2007; Taberner *et al.*, 2009; Wagner *et al.*, 2009). However, phosphorylation of Cdh1 did not enhance its binding to Msn5 (Jaquenoud *et al.*, 2002). Thus it remains open whether export of Cdh1 is regulated. Constitutive export combined with nuclear import during anaphase and G1 controlled by a potent, Cdk-inhibited NLS might explain the cell cycle–dependent localization of Cdh1.

After nuclear export, a portion of Cdh1 localized to the bud neck. This association was mediated by the C-terminal WD40 substrate-binding domain of Cdh1 (Figure 1, B and D). Even though certain substrates, such as Hsl1 and Iqg1, localize to this structure (Barral *et al.*, 1999; Burton and Solomon, 2000; Ko *et al.*, 2007), Cdh1 is unlikely to be active there because Cdh1 is phosphorylated at its

Cdk sites in the NTD and therefore inhibited for APC/C binding in this cell cycle stage. Moreover, localization studies failed to detect any APC/C at the bud neck (Zachariae, Shin, *et al.*, 1996; Melloy and Holloway, 2004). Finally, degradation of the bud neck localized substrate Iqg1 started in late anaphase (Arnold, Höckner, *et al.*, 2015), a stage at which Cdh1 has already left the bud neck and entered the nucleus. Thus ubiquitination by Cdh1 at the bud neck seems unlikely. Instead, localization to the bud neck might contribute to the regulation of Cdh1 by supporting cytoplasmic retention to reinforce exclusion of Cdh1 from the nucleus before anaphase.

Besides regulating nuclear localization via Cdk sites 1–3, we found that Cdk1 controls APC/C binding of Cdh1 by phosphorylation at Cdk sites 4–9, which are subdivided into two clusters. Of importance, phosphorylation of each cluster affected the APC/C-Cdh1 interaction, and simultaneous mutation of both clusters had an additive effect on Cdh1 binding to the APC/C (Figure 5C), raising the possibility that these two groups of Cdk sites regulate distinct APC/C interaction motifs in Cdh1. This idea receives support from a recent study that describes an atomic model of human APC/C-Cdh1 bound to its inhibitor Emi1 (Chang, Zhang, *et al.*, 2015). According to this model, the Cdh1 NTD makes multiple contacts to the APC/C subunits Apc8/Cdc23 and Apc1. Whereas the C-box and a conserved LF motif bind to Apc8/Cdc23, two α-helices interact with the PC domain of Apc1 through conserved hydrophobic residues, including the leucine residues of a KLLR motif, which resembles the KILR motif, identified as an APC/C binding site in human Cdc20 (Zhang and Lees, 2001; Izawa and Pines, 2012). Moreover, Chang, Zhang, *et al.* (2015) discovered that only four of the nine Cdk sites in human Cdh1 are critical for the negative regulation of APC/C-Cdh1 activity by phosphorylation. The atomic model revealed that two of these Cdk sites (serine 40 and threonine 121) reside at the interface to Apc8/Cdc23, whereas the other two sites (serines 151 and 163) are adjacent to the KLLR motif that contacts Apc1. Of note, the hydrophobic residues of the KLLR motif, as well as the flanking Cdk sites, which correspond to Cdk sites 8 and 9 in yeast Cdh1, are invariant in mammalian and yeast orthologues (Figure 7B). Although Cdk sites 4–7 of yeast Cdh1 are less conserved in their number and position, sequence alignment indicates that these sites are adjacent to the conserved LF motif, which makes contacts to Cdc23/Apc8 in human APC/C and may therefore be equivalent to threonine 121 of the human protein (Figure 7B). Thus APC/C binding sites, as well as their regulation by Cdk phosphorylation, seem to be conserved among Cdh1 orthologues.

Of interest, human Cdh1 contains a Cdk-inhibited NLS in its N-terminal domain like its orthologue in budding yeast (Zhou *et al.*, 2003a). However, the NLS of human Cdh1 is not located at the N-terminal end of the activator but instead comprises a 28–amino acid stretch adjacent to the WD40 domain and includes both the KLLR motif and the neighboring Cdk sites. This region was reported not only to be required for nuclear localization of human Cdh1 (Zhou *et al.*, 2003b), but also to be sufficient to drive heterologous GFP into the nucleus (Zhou *et al.*, 2003a). Thus, in the case of human Cdh1, the NLS overlaps with an APC/C binding site. In fact, the NLS of human Cdh1 is controlled by the same Cdk sites (Zhou *et al.*, 2003a), whose phosphorylation is also involved in preventing human Cdh1 from binding and activating the APC/C in vitro (Lukas *et al.*, 1999; Chang, Zhang, *et al.*, 2015). This appears different in budding yeast, since a segment comprising the KLLR-Cdk–site region of yeast Cdh1, residues 145–257, did not confer nuclear localization to GFP. In addition, none of the Cdk sites 4–9 located in this subdomain affected nuclear transport of Cdh1(1-257)-GFP. Despite these differences in the NLS location, the presence of a Cdk-inhibited NLS in human Cdh1 suggests that APC/C-Cdh1 activity in human cells might also be controlled at the level of Cdh1 localization. Indeed, phosphorylation of Cdh1 by Cdk5 under excitotoxic conditions was reported to cause accumulation of Cdh1 in the cytoplasm of postmitotic neurons, leading to increased cyclin B1 levels in the nucleus and subsequent cell death (Maestre *et al.*, 2008). Thus, at least in nondividing cells, Cdk-regulated nuclear localization of Cdh1 might provide spatial control of APC/C-Cdh1 activity in higher eukaryotes as well.

MATERIALS AND METHODS

Yeast strains and DNA constructs

All strains used in this study are derivatives of W303 and listed in Supplemental Table S1. Standard protocols were used for transformation, mating, sporulation, and tetrad dissection of yeast cells (Ausubel *et al.*, 2005). Yeast plasmid vectors are derivatives of pRS vectors (Sikorski and Hieter, 1989) or the disintegrator vector pIS375 (Sadowski *et al.*, 2007) and are listed in Supplemental Table S2. PCR was used to amplify and add restriction sites to genes or gene fragments for subsequent cloning. All constructs generated by PCR were verified by commercial DNA sequencing (Seqlab, Göttingen, Germany).

All *CDH1* constructs in this study are based on pWS203 (Schwab *et al.*, 1997). *CDH1* mutant alleles lacking potential Cdk phosphorylation sites due to replacement of the corresponding serine or threonine codons by alanine codons have been described (Zachariae, Schwab, *et al.*, 1998). New combinations of Cdk-site mutations were generated by exchanging gene segments between mutant and wild-type *CDH1* constructs using internal restriction sites. To generate the m(4-9)D mutation, a *CDH1* fragment in which the threonine and serine codons of Cdk sites at positions 157, 169, 173, 176, 227, and 239 were changed to aspartate codons was produced by commercial gene synthesis (Eurofins Genomics, Ebersberg, Germany). Internal *Xcm*I and *Cla*I sites were used to replace codons 74–283 of wild-type *CDH1* and *CDH1-m(1-3)A* with the equivalent codons of the synthesized fragment to produce *CDH1-m(4-9)D* or *CDH1-m(1-3)A-m(4-9)D*, respectively. Site-directed mutagenesis (Stratagene, La Jolla, CA) was used to replace the phosphoaccepting residues of Cdk sites 1–3 (T12, S16, and S42) with aspartate codons, creating *CDH1-m(1-3)D*. To inactivate the predicted NLS in the NTD of *CDH1* (NLSm1, NLSm2, and NLSm1,2), the lysine and arginine codons within the predicted sequence (Figure 3A) were changed to alanine codons by site-directed mutagenesis.

GFP fusion constructs of Cdh1 were created using a codon-optimized version of the *GFP* gene (Cormack *et al.*, 1997). In pWS2793 and pWS4085, the *GFP* gene was amplified by PCR and cloned between the *TEF2* promoter and the *CYC1* terminator in pRS306. The *TEF2* promoter was PCR amplified from yeast genomic DNA (445 base pairs upstream to the *TEF2* open reading frame) and the *CYC1* terminator derived from p414-GAL1 (Mumberg *et al.*, 1994). *CDH1* truncation constructs encoding the Cdh1 NTD were generated by PCR using pWS203 as a template and cloned between the *TEF2* promoter and the *GFP* gene in pWS4085. To produce *CDH1* truncation constructs bearing mutations in Cdk phosphorylation sites or the predicted NLS, plasmid vectors that contain the respective mutant allele of *CDH1* were used as PCR templates. *CDH1*(codons 245-566) encoding the CTD were PCR amplified from pWS203 and fused to the 3′ end of the *GFP* gene in pWS2793. In pWS4667, the *CDH1* gene was first amplified by PCR from pWS203 and cloned to the 3′ end of the *GFP* gene in pWS2793, and the *TEF2* promoter was then replaced by the *MET25* promoter of p413-MET25 (Mumberg *et al.*, 1994). In pWS4721 and pWS4722, wild-type *CDH1* was

replaced by *CDH1-m(1-3)A* and *CDH1-m(4-9)A* constructs, respectively. All GFP fusion constructs were integrated at the *URA3* locus.

For coimmunoprecipitation analysis, full-length *CDH1* constructs containing mutations in Cdk sites were fused to *pGALL-HA3* by replacing wild-type *CDH1* in pWS383 (*pGALL-HA3-CDH1-tCYC1* in pRS306 (Schwab *et al.*, 2001). The resulting *pGALL-HA3*-constructs were then cloned into the disintegrator plasmid pIS375 to enable selection for single-copy integrations as described (Sadowski *et al.*, 2007). In brief, pIS375 contains a *URA3* marker gene, as well as Yip-In and Yip-Out elements, which are the flanking sequences of the yeast genomic *MET15* gene. *pGALL-HA3-CDH1* constructs were cloned between the Yip-In and Yip-out elements, which produce duplicated sequences after integration of the plasmids at the *MET15* locus via the Yip-In element. Transformed cells were selected on synthetic complete (SC)-uracil plates (3 d, 30°C). Selected colonies were first restreaked onto SC-uracil plates (2 d, 30°C) and subsequently onto yeast extract/peptone/dextrose plates (4 d, 25°C) to allow recombination within the integrated plasmid construct under nonselective conditions. Colonies were then restreaked twice in a row onto SC plates supplemented with 1 mg/ml 5-fluoroorotic acid (Zymo Research, Irvine, CA) to select for recombination-mediated loss of the URA3 marker gene. Recombination events resulted in either complete loss of the integrated plasmid or single-copy integration of the *pGALL-HA3-CDH1* construct within the disrupted *MET15* gene. Clones bearing single-copy integrations were identified by replica plating on SC-methionine plates and verified by Western analysis.

The *CDC23-MYC9* construct and the nuclear Cherry marker have been described (Zachariae, Shin, *et al.*, 1996; Arnold, Höckner, *et al.*, 2015). Endogenous *CDC23* was tagged with GFP using a PCR-based epitope tagging method described previously (Sheff and Thorn, 2004). To create endogenously expressed *CDC11-3mCherry*, the *CDC11* gene was PCR amplified from yeast genomic DNA and fused to the 5′ end of the *3mCherry* construct (Shaner *et al.*, 2004) in pRS305. The resulting plasmid (pWS3124) was integrated at the *CDC11* locus.

Media, growth conditions, and cell cycle arrest

Cells were grown at 25°C in yeast extract/peptone (YEP) complex medium containing adenine (100 mg/l), tryptophan (200 mg/l), and KH_2PO_4 (10 mM) supplemented with 2% glucose or 2% raffinose. To induce expression of *GFP-CDH1* constructs from the *MET25* promoter, exponentially growing cells cultivated in glucose-containing YEP medium were harvested by centrifugation, washed once in synthetic medium lacking methionine, and then cultivated in synthetic medium lacking methionine for 45 min. For low-level, constitutive expression from the *MET25* promoter, cells were cultivated in synthetic medium supplemented with 100 µM methionine. To induce expression of *HA3-CDH1* constructs from the *GALL* promoter or *CLB2-db* from the *GAL1-10* promoter, galactose (2%) was added for 2 h to exponentially growing cells cultivated in YEP medium containing raffinose. For cell cycle arrest in metaphase, cells were incubated in the presence of 7.5 µg/ml nocodazole (AppliChem, Darmstadt, Germany) for 3 h.

Fluorescence microscopy

For live-cell imaging, exponentially growing cells were harvested by centrifugation, transferred onto a coverslip, and covered with an agarose pad (0.75% agarose) supplied with amino acids, yeast nitrogen base, and glucose (2%). Cells were imaged at 21–22.5°C using a Plan Apochromat 63×/1.40 oil differential interference contrast (DIC) M27 lens on an Observer Z.1 microscope (Carl Zeiss, Jena, Germany) equipped with a CSU-X1 confocal spinning-disk unit (Yokogawa, Tokyo, Japan) and an AxioCam MRm camera (Carl Zeiss). *Z*-stacks with 10 slices at 0.5-µm distance were taken with an exposure time of 200 ms for each channel. For time-lapse images, *Z*-stacks were taken at 5-min intervals for 2 h.

Data processing and quantification were done with ImageJ (National Institutes of Health, Bethesda, MD). To compile images or movies, *Z*-stacks were projected using median-intensity projection for the DIC channel or maximum-intensity projection with subsequent contrast enhancement for fluorescence channels. A region of interest (ROI) was selected and duplicated for each channel, fluorescence channels were merged, and single images were combined using the stack-combiner plug-in.

Nuclear GFP intensities were quantified in nonprojected fluorescence channels using the three-dimensional (3D) manager plug-in (Ollion *et al.*, 2013). To this end, an identical area without cells or fluorescence signal was selected for both fluorescence channels and used for subtraction of background applying the "background subtraction from ROI" command of the ROI plug-in (number of SD from mean = 0). An identical area containing the cell of interest was defined in each channel and duplicated as a hyperstack consisting of *Z*-slices and time frames. For each channel, the duplicated hyperstack was split into single time frames, and the resulting *Z*-stacks were then assembled in chronological order into one combined *Z*-stack. To automatically recognize and load nuclear signals as ROIs into the 3D manager, a median filter (radius 3.0) and subsequently an automatic threshold (MaxEntropy) were applied to the combined *Z*-stack displaying the nuclear Cherry marker, and then the "3D segmentation" function of the 3D manager plug-in was used to label nuclear signals as ROIs. After addition to the 3D manager, the ROIs were applied to the combined *Z*-stack of the GFP channel, and nuclear GFP intensities were measured using the "Quantify 3D" function of the 3D manager plug-in.

Protein analysis

For preparation of whole-cell extracts (WCEs), exponentially growing cells were harvested by centrifugation, washed once with ice-cold water, and resuspended in ice-cold lysis buffer (150 mM NaCl, 50 mM Tris-HCl, pH 7.5, 5 mM EDTA, 0.1% IGEPAL CA-630). Optionally, lysis buffer was supplemented with 50 mM NaF and 60 mM β-glycerol phosphate to inhibit phosphatase activity during extract preparation (Figures 5 and 6 and Supplemental Figures S3 and S6). An equal volume of glass beads was added to the cell suspension, and cells were broken in a mixer mill (Retsch, Haan, Germany) for 5 min at 4°C. Cell debris and glass beads were removed by centrifugation at 4°C. For analysis of WCEs, the supernatant was mixed with an equal volume of 2× Laemmli sample buffer and boiled for 10 min at 100°C. For immunoprecipitation of HA3-tagged Cdh1 derivatives, WCEs were incubated with mouse monoclonal anti-HA antibody (12CA5) for 2 h at 4°C. Protein A–agarose beads were added, and the mixtures were rotated for an additional 2 h at 4°C. Beads were collected by centrifugation, washed three times with ice-cold lysis buffer, and boiled in Laemmli sample buffer for 10 min at 100°C.

Proteins were separated on a 9% SDS–PAGE gel and blotted on a nitrocellulose membrane by standard semidry Western blotting. 12CA5 antibody was used to detect HA-tagged Cdh1 proteins. Cdc23-Myc9 was detected with mouse monoclonal anti-Myc antibody 9E10 or rabbit polyclonal anti-Myc antibody A-14 (Santa Cruz Biotechnology, Dallas, TX; Supplemental Figure S3). GFP fusion proteins were detected with mouse monoclonal GFP antibody (Roche, Indianapolis, IN). Endogenous Gcd11, Tub2, and Clb2, as

well as Clb2-db, were probed with specific polyclonal rabbit antisera. Goat anti-mouse IRDye800 and goat anti-rabbit IRDye680 antibodies (LI-COR Biosciences, Bad Homburg, Germany) were used as secondary antibodies, and immunoblots were analyzed with an Odyssey Infrared Imaging System (LI-COR Biosciences).

To quantify the fluorescence intensities of detected signals, integrated density plots were produced using the gel analyzer function of ImageJ. To this end, lanes of interest were marked in their whole length using the rectangle tool. The width of the marking rectangle was smaller than the width of the smallest band quantified. After generation of the profile plots, a line was drawn within the plotted peaks at the level of the integrated background to perform a baseline subtraction. The areas of such enclosed peaks were then measured using the wand tool. Quantification of Clb2 signals in WCEs and Cdc23-Myc9 signals in coimmunoprecipitates are shown in histograms. For the Clb2 histogram, Clb2 signal intensities were calculated and normalized to the corresponding Gcd11 signals, and the value for the control strain was set to 1. For the Cdc23-Myc9 histogram, signal intensities of coprecipitated Cdc23-Myc9 were measured, adjusted for Cdh1 recovery, and then normalized to wild-type Cdh1 (WT = 1).

ACKNOWLEDGMENTS

We thank Alexander Bauer, Andrea Brücher, Antje Machetanz-Morokane, and Adelheid Weissgerber for technical assistance and Frank Sprenger for help with microscopy. S.H. was supported by a PhD Fellowship from the Elitenetzwerk Bayern.

REFERENCES

Boldface names denote co–first authors.

Almeida A (2012). Regulation of APC/C-Cdh1 and its function in neuronal survival. Mol Neurobiol 46, 547–554.

Almeida A, Bolanos JP, Moreno S (2005). Cdh1/Hct1-APC is essential for the survival of postmitotic neurons. J Neurosci 25, 8115–8121.

Arnold L, Höckner S, Seufert W (2015). Insights into the cellular mechanism of the yeast ubiquitin ligase APC/C-Cdh1 from the analysis of in vivo degrons. Mol Biol Cell 26, 843–858.

Ausubel F, Brent R, Kingston R, Moore D, Seidman J, Smith J, Struhl K (2005). Current Protocols in Molecular Biology, New York: John Wiley & Sons.

Barford D (2011). Structural insights into anaphase-promoting complex function and mechanism. Philos Trans R Soc Lond B Biol Sci 366, 3605–3624.

Barral Y, Parra M, Bidlingmaier S, Snyder M (1999). Nim1-related kinases coordinate cell cycle progression with the organization of the peripheral cytoskeleton in yeast. Genes Dev 13, 176–187.

Bassermann F, Eichner R, Pagano M (2014). The ubiquitin proteasome system - implications for cell cycle control and the targeted treatment of cancer. Biochim Biophys Acta 1843, 150–162.

Blanco MA, Sanchez-Diaz A, de Prada JM, Moreno S (2000). APC(ste9/srw1) promotes degradation of mitotic cyclins in G(1) and is inhibited by cdc2 phosphorylation. EMBO J 19, 3945–3955.

Bloom J, Cross FR (2007). Multiple levels of cyclin specificity in cell-cycle control. Nat Rev Mol Cell Biol 8, 149–160.

Boustany LM, Cyert MS (2002). Calcineurin-dependent regulation of Crz1p nuclear export requires Msn5p and a conserved calcineurin docking site. Genes Dev 16, 608–619.

Brandeis M, Hunt T (1996). The proteolysis of mitotic cyclins in mammalian cells persists from the end of mitosis until the onset of S phase. EMBO J 15, 5280–5289.

Burton JL, Solomon MJ (2000). Hsl1p, a Swe1p inhibitor, is degraded via the anaphase-promoting complex. Mol Cell Biol 20, 4614–4625.

Chang L, Zhang Z, Yang J, McLaughlin SH, Barford D (2014). Molecular architecture and mechanism of the anaphase-promoting complex. Nature 513, 388–393.

Chang L, Zhang Z, Yang J, McLaughlin SH, Barford D (2015). Atomic structure of the APC/C and its mechanism of protein ubiquitination. Nature 522, 450–454.

Chao WC, Kulkarni K, Zhang Z, Kong EH, Barford D (2012). Structure of the mitotic checkpoint complex. Nature 484, 208–213.

Clute P, Pines J (1999). Temporal and spatial control of cyclin B1 destruction in metaphase. Nat Cell Biol 1, 82–87.

Cohen-Fix O, Peters JM, Kirschner MW, Koshland D (1996). Anaphase initiation in Saccharomyces cerevisiae is controlled by the APC-dependent degradation of the anaphase inhibitor Pds1p. Genes Dev 10, 3081–3093.

Cormack BP, Bertram G, Egerton M, Gow NA, Falkow S, Brown AJ (1997). Yeast-enhanced green fluorescent protein (yEGFP): a reporter of gene expression in Candida albicans. Microbiology 143, 303–311.

Deshaies RJ, Ferrell JE Jr (2001). Multisite phosphorylation and the countdown to S phase. Cell 107, 819–822.

DeVit MJ, Johnston M (1999). The nuclear exportin Msn5 is required for nuclear export of the Mig1 glucose repressor of Saccharomyces cerevisiae. Curr Biol 9, 1231–1241.

Eguren M, Manchado E, Malumbres M (2011). Non-mitotic functions of the Anaphase-Promoting Complex. Semin Cell Dev Biol 22, 572–578.

Enserink JM, Kolodner RD (2010). An overview of Cdk1-controlled targets and processes. Cell Div 5, 11.

Ferrell JE Jr, Ha SH (2014). Ultrasensitivity part II: multisite phosphorylation, stoichiometric inhibitors, and positive feedback. Trends Biochem Sci 39, 556–569.

Glotzer M, Murray AW, Kirschner MW (1991). Cyclin is degraded by the ubiquitin pathway. Nature 349, 132–138.

Hall MC, Warren EN, Borchers CH (2004). Multi-kinase phosphorylation of the APC/C activator Cdh1 revealed by mass spectrometry. Cell Cycle 3, 1278–1284.

He J, Chao WC, Zhang Z, Yang J, Cronin N, Barford D (2013). Insights into degron recognition by APC/C coactivators from the structure of an Acm1-Cdh1 complex. Mol Cell 50, 649–660.

Herzog F, Primorac I, Dube P, Lenart P, Sander B, Mechtler K, Stark H, Peters JM (2009). Structure of the anaphase-promoting complex/cyclosome interacting with a mitotic checkpoint complex. Science 323, 1477–1481.

Holt LJ, Tuch BB, Villén J, Johnson AD, Gygi SP, Morgan DO (2009). Global analysis of Cdk1 substrate phosphorylation sites provides insights into evolution. Science 325, 1682–1686.

Irniger S, Nasmyth K (1997). The anaphase-promoting complex is required in G1 arrested yeast cells to inhibit B-type cyclin accumulation and to prevent uncontrolled entry into S-phase. J Cell Sci 110, 1523–1531.

Izawa D, Pines J (2012). Mad2 and the APC/C compete for the same site on Cdc20 to ensure proper chromosome segregation. J Cell Biol 199, 27–37.

Jaquenoud M, van Drogen F, Peter M (2002). Cell cycle-dependent nuclear export of Cdh1p may contribute to the inactivation of APC/C(Cdh1). EMBO J 21, 6515–6526.

Jaspersen SL, Charles JF, Morgan DO (1999). Inhibitory phosphorylation of the APC regulator Hct1 is controlled by the kinase Cdc28 and the phosphatase Cdc14. Curr Biol 9, 227–236.

Kaffman A, Rank NM, O'Neill EM, Huang LS, O'Shea EK (1998). The receptor Msn5 exports the phosphorylated transcription factor Pho4 out of the nucleus. Nature 396, 482–486.

Kelly A, Wickliffe KE, Song L, Fedrigo I, Rape M (2014). Ubiquitin chain elongation requires E3-dependent tracking of the emerging conjugate. Mol Cell 56, 232–245.

Kimata Y, Baxter JE, Fry AM, Yamano H (2008). A role for the Fizzy/Cdc20 family of proteins in activation of the APC/C distinct from substrate recruitment. Mol Cell 32, 576–583.

King RW, Deshaies RJ, Peters JM, Kirschner MW (1996). How proteolysis drives the cell cycle. Science 274, 1652–1659.

Ko N, Nishihama R, Tully GH, Ostapenko D, Solomon MJ, Morgan DO, Pringle JR (2007). Identification of yeast IQGAP (Iqg1p) as an anaphase-promoting-complex substrate and its role in actomyosin-ring-independent cytokinesis. Mol Biol Cell 18, 5139–5153.

Koivomägi M, Ord M, Iofik A, Valk E, Venta R, Faustova I, Kivi R, Balog ER, Rubin SM, Loog M (2013). Multisite phosphorylation networks as signal processors for Cdk1. Nat Struct Mol Biol 20, 1415–1424.

Koivomägi M, Valk E, Venta R, Iofik A, Lepiku M, Balog ER, Rubin SM, Morgan DO, Loog M (2011). Cascades of multisite phosphorylation control Sic1 destruction at the onset of S phase. Nature 480, 128–131.

Kosugi S, Hasebe M, Entani T, Takayama S, Tomita M, Yanagawa H (2008). Design of peptide inhibitors for the importin alpha/beta nuclear import pathway by activity-based profiling. Chem Biol 15, 940–949.

Kosugi S, Hasebe M, Tomita M, Yanagawa H (2009). Systematic identification of cell cycle-dependent yeast nucleocytoplasmic shuttling proteins by prediction of composite motifs. Proc Natl Acad Sci USA 106, 10171–10176.

Kraft C, Herzog F, Gieffers C, Mechtler K, Hagting A, Pines J, Peters JM (2003). Mitotic regulation of the human anaphase-promoting complex by phosphorylation. EMBO J 22, 6598–6609.

Kraft C, Vodermaier HC, Maurer-Stroh S, Eisenhaber F, Peters JM (2005). The WD40 propeller domain of Cdh1 functions as a destruction box receptor for APC/C substrates. Mol Cell 18, 543–553.
Kramer ER, Scheuringer N, Podtelejnikov AV, Mann M, Peters JM (2000). Mitotic regulation of the APC activator proteins CDC20 and CDH1. Mol Biol Cell 11, 1555–1569.
Kulak NA, Pichler G, Paron I, Nagaraj N, Mann M (2014). Minimal, encapsulated proteomic-sample processing applied to copy-number estimation in eukaryotic cells. Nat Methods 11, 319–324.
Kutay U, Guttinger S (2005). Leucine-rich nuclear-export signals: born to be weak. Trends Cell Biol 15, 121–124.
Labit H, Fujimitsu K, Bayin NS, Takaki T, Gannon J, Yamano H (2012). Dephosphorylation of Cdc20 is required for its C-box-dependent activation of the APC/C. EMBO J 31, 3351–3362.
Liku ME, Nguyen VQ, Rosales AW, Irie K, Li JJ (2005). CDK phosphorylation of a novel NLS-NES module distributed between two subunits of the Mcm2-7 complex prevents chromosomal rereplication. Mol Biol Cell 16, 5026–5039.
Lukas C, Sorensen CS, Kramer E, Santoni-Rugiu E, Lindeneg C, Peters JM, Bartek J, Lukas J (1999). Accumulation of cyclin B1 requires E2F and cyclin-A-dependent rearrangement of the anaphase-promoting complex. Nature 401, 815–818.
Maestre C, Delgado-Esteban M, Gomez-Sanchez JC, Bolanos JP, Almeida A (2008). Cdk5 phosphorylates Cdh1 and modulates cyclin B1 stability in excitotoxicity. EMBO J 27, 2736–2745.
Martinez JS, Hall H, Bartolowits MD, Hall MC (2012). Acm1 contributes to nuclear positioning by inhibiting Cdh1-substrate interactions. Cell Cycle 11, 384–394.
Martinez JS, Jeong DE, Choi E, Billings BM, Hall MC (2006). Acm1 is a negative regulator of the CDH1-dependent anaphase-promoting complex/cyclosome in budding yeast. Mol Cell Biol 26, 9162–9176.
McGrath DA, Balog ER, Koivomägi M, Lucena R, Mai MV, Hirschi A, Kellogg DR, Loog M, Rubin SM (2013). Cks confers specificity to phosphorylation-dependent CDK signaling pathways. Nat Struct Mol Biol 20, 1407–1414.
Melloy PG, Holloway SL (2004). Changes in the localization of the Saccharomyces cerevisiae anaphase-promoting complex upon microtubule depolymerization and spindle checkpoint activation. Genetics 167, 1079–1094.
Moll T, Tebb G, Surana U, Robitsch H, Nasmyth K (1991). The role of phosphorylation and the CDC28 protein kinase in cell cycle-regulated nuclear import of the S. cerevisiae transcription factor SWI5. Cell 66, 743–758.
Mumberg D, Muller R, Funk M (1994). Regulatable promoters of Saccharomyces cerevisiae: comparison of transcriptional activity and their use for heterologous expression. Nucleic Acids Res 22, 5767–5768.
O'Conallain C, Doolin MT, Taggart C, Thornton F, Butler G (1999). Regulated nuclear localisation of the yeast transcription factor Ace2p controls expression of chitinase (CTS1) in Saccharomyces cerevisiae. Mol Gen Genet 262, 275–282.
Ollion J, Cochennec J, Loll F, Escude C, Boudier T (2013). TANGO: a generic tool for high-throughput 3D image analysis for studying nuclear organization. Bioinformatics 29, 1840–1841.
Pesin JA, Orr-Weaver TL (2008). Regulation of APC/C activators in mitosis and meiosis. Annu Rev Cell Dev Biol 24, 475–499.
Peters JM (2006). The anaphase promoting complex/cyclosome: a machine designed to destroy. Nat Rev Mol Cell Biol 7, 644–656.
Petroski MD, Deshaies RJ (2005). Function and regulation of cullin-RING ubiquitin ligases. Nat Rev Mol Cell Biol 6, 9–20.
Pfleger CM, Kirschner MW (2000). The KEN box: an APC recognition signal distinct from the D box targeted by Cdh1. Genes Dev 14, 655–665.
Pines J (1999). Four-dimensional control of the cell cycle. Nat Cell Biol 1, E73–79.
Primorac I, Musacchio A (2013). Panta rhei: the APC/C at steady state. J Cell Biol 201, 177–189.
Rudner AD, Murray AW (2000). Phosphorylation by Cdc28 activates the Cdc20-dependent activity of the anaphase-promoting complex. J Cell Biol 149, 1377–1390.
Sadowski I, Su TC, Parent J (2007). Disintegrator vectors for single-copy yeast chromosomal integration. Yeast 24, 447–455.
Schwab M, Lutum AS, Seufert W (1997). Yeast Hct1 is a regulator of Clb2 cyclin proteolysis. Cell 90, 683–693.
Schwab M, Neutzner M, Mocker D, Seufert W (2001). Yeast Hct1 recognizes the mitotic cyclin Clb2 and other substrates of the ubiquitin ligase APC. EMBO J 20, 5165–5175.
Shaner NC, Campbell RE, Steinbach PA, Giepmans BN, Palmer AE, Tsien RY (2004). Improved monomeric red, orange and yellow fluorescent proteins derived from Discosoma sp. red fluorescent protein. Nat Biotechnol 22, 1567–1572.
Sheff MA, Thorn KS (2004). Optimized cassettes for fluorescent protein tagging in Saccharomyces cerevisiae. Yeast 21, 661–670.
Shirayama M, Toth A, Galova M, Nasmyth K (1999). APC(Cdc20) promotes exit from mitosis by destroying the anaphase inhibitor Pds1 and cyclin Clb5. Nature 402, 203–207.
Sidorova JM, Mikesell GE, Breeden LL (1995). Cell cycle-regulated phosphorylation of Swi6 controls its nuclear localization. Mol Biol Cell 6, 1641–1658.
Sikorski RS, Hieter P (1989). A system of shuttle vectors and yeast host strains designed for efficient manipulation of DNA in Saccharomyces cerevisiae. Genetics 122, 19–27.
Sivakumar S, Gorbsky GJ (2015). Spatiotemporal regulation of the anaphase-promoting complex in mitosis. Nat Rev Mol Cell Biol 16, 82–94.
Sullivan M, Morgan DO (2007). Finishing mitosis, one step at a time. Nat Rev Mol Cell Biol 8, 894–903.
Swaney DL, Beltrao P, Starita L, Guo A, Rush J, Fields S, Krogan NJ, Villen J (2013). Global analysis of phosphorylation and ubiquitylation cross-talk in protein degradation. Nat Methods 10, 676–682.
Taberner FJ, Quilis I, Igual JC (2009). Spatial regulation of the start repressor Whi5. Cell Cycle 8, 3010–3018.
Teixeira LK, Reed SI (2013). Ubiquitin ligases and cell cycle control. Annu Rev Biochem 82, 387–414.
Tian W, Li B, Warrington R, Tomchick DR, Yu H, Luo X (2012). Structural analysis of human Cdc20 supports multisite degron recognition by APC/C. Proc Natl Acad Sci USA 109, 18419–18424.
Ueta R, Fujiwara N, Iwai K, Yamaguchi-Iwai Y (2007). Mechanism underlying the iron-dependent nuclear export of the iron-responsive transcription factor Aft1p in Saccharomyces cerevisiae. Mol Biol Cell 18, 2980–2990.
Van Voorhis VA, Morgan DO (2014). Activation of the APC/C ubiquitin ligase by enhanced E2 efficiency. Curr Biol 24, 1556–1562.
Vodermaier HC, Gieffers C, Maurer-Stroh S, Eisenhaber F, Peters JM (2003). TPR subunits of the anaphase-promoting complex mediate binding to the activator protein CDH1. Curr Biol 13, 1459–1468.
Wagner MV, Smolka MB, de Bruin RA, Zhou H, Wittenberg C, Dowdy SF (2009). Whi5 regulation by site specific CDK-phosphorylation in Saccharomyces cerevisiae. PLoS One 4, e4300.
Waizenegger IC, Hauf S, Meinke A, Peters JM (2000). Two distinct pathways remove mammalian cohesin from chromosome arms in prophase and from centromeres in anaphase. Cell 103, 399–410.
Wasch R, Cross FR (2002). APC-dependent proteolysis of the mitotic cyclin Clb2 is essential for mitotic exit. Nature 418, 556–562.
Wurzenberger C, Gerlich DW (2011). Phosphatases: providing safe passage through mitotic exit. Nat Rev Mol Cell Biol 12, 469–482.
Yeong FM, Lim HH, Padmashree CG, Surana U (2000). Exit from mitosis in budding yeast: biphasic inactivation of the Cdc28-Clb2 mitotic kinase and the role of Cdc20. Mol Cell 5, 501–511.
Zachariae W, Schwab M, Nasmyth K, Seufert W (1998). Control of cyclin ubiquitination by CDK-regulated binding of Hct1 to the anaphase promoting complex. Science 282, 1721–1724.
Zachariae W, Shin TH, Galova M, Obermaier B, Nasmyth K (1996). Identification of subunits of the anaphase-promoting complex of Saccharomyces cerevisiae. Science 274, 1201–1204.
Zhang Y, Lees E (2001). Identification of an overlapping binding domain on Cdc20 for Mad2 and anaphase-promoting complex: model for spindle checkpoint regulation. Mol Cell Biol 21, 5190–5199.
Zhou Y, Ching YP, Chun AC, Jin DY (2003a). Nuclear localization of the cell cycle regulator CDH1 and its regulation by phosphorylation. J Biol Chem 278, 12530–12536.
Zhou Y, Ching YP, Ng RW, Jin DY (2003b). Differential expression, localization and activity of two alternatively spliced isoforms of human APC regulator CDH1. Biochem J 374, 349–358.